NATIONAL ADVISORY COMMITTEE FOR AERONAUTICS

TECHNICAL NOTE 2659

A MINIATURE ELECTRICAL PRESSURE GAGE UTILIZING A STRETCHED FLAT DIAPHRAGM

By John L. Patterson

Langley Aeronautical Laboratory
Langley Field, Va.

Washington
April 1952

NATIONAL ADVISORY COMMITTEE FOR AERONAUTICS

TECHNICAL NOTE 2659

A MINIATURE ELECTRICAL PRESSURE GAGE UTILIZING A STRETCHED FLAT DIAPHRAGM

By John L. Patterson

SUMMARY

A variable-air-gap inductance type of electrical pressure gage is described that is basically 7/16 inch in diameter and 1/4 inch in thickness. The gage was designed to measure pressures fluctuating at high frequencies. It is also capable of measuring steady-state pressures with errors of less than 1 percent of full scale and has proved to be of value as a general-purpose electrical gage for aeronautical work where small size and minimum response to acceleration forces are important factors.

Design equations and curves are presented which can be used to predict the deflections and fundamental natural frequencies of stretched flat diaphragms.

INTRODUCTION

In recent aeronautical research where the trend is to higher airspeeds, the measurement of fluctuating pressures has become more essential and at the same time more difficult. The measurements are more essential because air-flow disturbances such as buffeting become more pronounced with increase in Mach number. They are difficult because, in general, pressures fluctuate at high frequencies, temperature changes are wide, and accelerations are violent. In addition, high-speed airfoils are thin, and models installed in high-speed tunnels are often quite small.

For some time these trends have indicated an urgent need for electrical pressure gages which will satisfy the following basic requirements:

(1) Very small size: It is often necessary to mount the gage near the pressure orifice in small models to minimize the effect of connecting tubing on the gage response.

(2) Good frequency response to several thousand cycles per second: Very high mechanical resonant frequencies and either a flush diaphragm or very high acoustical resonant frequencies are thus required.

(3) Minimum response to accelerating forces: Vibratory accelerations of 100g or more and centrifugal accelerations of 5000g or more (on rotating devices such as propellers) may be expected.

(4) Minimum temperature effects: Temperatures from -50° F to 200° F may be expected.

(5) Sensitivity at low pressures: Lowest full-scale range should be ±1 pound per square inch or less; other ranges, up to ±100 pounds per square inch.

(6) Low internal impedance: Mounting space and conditions often prohibit the use of a preamplifier or other impedance-changing device.

(7) Linear variation of pressure with output voltage: This characteristic simplifies data reduction, especially where the pressures are varying in a complex manner.

(8) Convenient output: The output should be such that amplifying and recording equipment of standard design can be used.

(9) Simple and rugged construction: The construction should be such that the cost of construction and upkeep is minimized.

It was found that many desired fluctuating pressure measurements were difficult if not impossible to make with commercially available gages. In addition to their large size, many electrical gages built to measure low pressures have a rather low natural frequency and are often sensitive to acceleration forces. Piezoelectric-crystal-type gages have very good high-frequency response, but they are high-impedance devices and are vibration-sensitive. In addition, they cannot be used to measure steady-state or slowly changing pressures.

The miniature gage described in this paper, designated the NACA miniature electrical pressure gage model 49, was designed at the Instrument Research Division of the Langley Aeronautical Laboratory and has been found to meet many of the preceding requirements. Some of its uses at Langley have been the measurement of fluctuations in wind-tunnel flow, of pressure time histories in blowdown tunnels and shock tubes, of pressure distributions on oscillating models, and of fluctuating pressures in propeller studies and in buffeting investigations.

SYMBOLS

General:

A	area, square inches
a	linear acceleration, inches per second^2
E	Young's modulus of elasticity, pounds per inch^2
e	maximum tensile strain, inches per inch
e_o	strain due to initial diaphragm tension, inches per inch
f_a	acoustical natural frequency, cycles per second
g	acceleration due to gravity, inches per second^2
l	length, inches
p	pressure, pounds per inch^2
p_o	initial steady-state absolute pressure, pounds per inch^2
R	radius, inches
s	volume, inch^3
T	absolute temperature, degrees Rankine
t	thickness, inches
V_c	speed of sound, inches per second
W	deflection of diaphragm at center, inches
γ	ratio of specific heats
ζ	damping ratio
μ	absolute viscosity, pound-seconds per inch^2
ρ	density, pounds per inch^3
σ	Poisson's ratio
ω	frequency, radians per second $(2\pi f)$

ω_a acoustical natural frequency of the gage, radians per second

ω_m mechanical natural frequency of the diaphragm, radians per second

Electrical:

$j = \sqrt{-1}$

L inductance, henries

l_1 effective length of the magnetic flux path in metal, inches

l_2 length of the air gap, inches

R resistance, ohms

R_e effective alternating-current resistance, ohms

R_L load resistance, ohms

V_i input voltage, volts

V_o output voltage, volts

Z impedance, ohms

μ_o initial permeability

DESIGN CONSIDERATIONS

General Design Features

The variable-air-gap inductance type of electrical sensing element was selected because it was found to permit the closest approximation to the requirements listed in the introduction. For extreme compactness, the gage components are arranged as shown in figure 1. A flat, stretched, metal diaphragm is soldered between two cup-shaped metal case halves, each of which has a pressure opening and a core piece. An inductance coil is cemented about each core piece. The difference between the pressures in the two pressure openings causes the diaphragm to deflect so that the lengths of the air gaps between the diaphragm and core pieces are changed and thus the impedances of the coils are changed. The coils are connected in adjacent arms of an alternating-current Wheatstone bridge circuit so that a voltage output is produced proportional to the impedance changes. In this manner, a reasonable output can be obtained

by utilizing the small deflections of the miniature diaphragms $\left(\frac{5}{16}\text{-inch free diameter}\right)$ without decreasing their natural frequencies with added weight or mechanical linkages.

An inductance-type gage with small coils is an inherently low-impedance device which minimizes stray voltage pickup and permits long lead wires between the gage and its associated equipment. The use of two air gaps, one on each side of the diaphragm, results in increased and more linear output as is described subsequently. The double-air-gap type of gage also permits a symmetrical mechanical and electrical construction which reduces zero drift with temperature changes. Maintaining reasonable tolerances during the case-machining and coil-winding operations was found to make the zero drift quite small.

In order to minimize changes of diaphragm initial tension with temperature and hence changes of gage sensitivity, the case and diaphragm materials should have the same coefficient of expansion. In order to reduce changes in initial tension further, and to minimize temperature errors due to changes of air-gap dimensions, the coefficient of expansion should be small. The gage must be made of a magnetic material having a reasonably high initial permeability (as explained subsequently), and the thermoelastic coefficient of the diaphragm material should be small. Since the range of nickel-iron alloys between 35-percent and 50-percent nickel content meet many of these requirements, several such alloys were used to build experimental gages. The alloy having 42-percent nickel content was found to be the most suitable material available in the required diaphragm thicknesses and is used, in the fully annealed condition, for both the diaphragms and cases. Figure 2 shows how some of the critical characteristics vary with percent nickel content according to information supplied by the Carpenter Steel Company.

A pressure gage for general use should be able to withstand abuse, especially if it is to be built into a model. The NACA miniature electrical pressure gage has been found to meet this requirement because of its compact sturdy construction. The 42-percent nickel alloy has been found to be sufficiently corrosion resistant under the normal conditions to which the gages have been exposed at the Langley Laboratory, including contact with sea water.

Diaphragm Deflection

Reference 1 gives the following formulas for the bending of a flat stretched circular diaphragm, having its edges completely fixed, and where it can be assumed that $W < 8t$ and $e_o < \frac{10t^2}{R^2}$:

$$p = \frac{16}{3}\frac{Et^3W}{(1-\sigma^2)R^4}\left[1 + \frac{5(1+\sigma)}{6}e_o\frac{R^2}{t^2} + \frac{(1+\sigma)(173-73\sigma)}{360}\frac{W^2}{t^2}\right] \quad (1)$$

$$e - e_o = \frac{4Wt}{R^2}\left[1 + \frac{1+\sigma}{3}e_o\frac{R^2}{t^2} + \frac{W}{12t} + \frac{(1+\sigma)(83-43\sigma)}{360}\frac{W^2}{t^2}\right] \quad (2)$$

When the following constant values for the NACA miniature gage are put into these relations:

$$R = \frac{5}{32} \text{ inch}$$

$$E = 22 \times 10^6 \text{ pounds per inch}^2$$

$$\sigma = 0.29$$

equation (1) becomes

$$p = 21.49 \times 10^{10}t^3W\left(1 + 0.0263\frac{e_o}{t^2} + 0.544\frac{W^2}{t^2}\right) \quad (3)$$

and equation (2) becomes

$$e - e_o = 163.8Wt\left(1 + 0.0105\frac{e_o}{t^2} + \frac{W}{12t} + 0.253\frac{W^2}{t^2}\right) \quad (4)$$

It is apparent from equation (3) that, when the deflection W is of the same order of magnitude as the thickness t and there is no initial tension e_o, the pressure-deflection curve will be quite nonlinear. A widely used method of reducing this nonlinearity by corrugating the diaphragm becomes impractical where small size and high natural frequency are important considerations. In this design it was decided to improve linearity by applying enough initial tension so that, in equation (3):

$$1 + 0.0263\frac{e_o}{t^2} \gg 0.544\frac{W^2}{t^2}$$

Initial tension also considerably reduces the effects of the small distortions usually present in thin diaphragm materials.

If the maximum allowed nonlinearity be defined as a 1-percent deviation from the straight-line portion (near the origin) of the pressure-deflection curve, the following expression is obtained from equation (3):

$$1 + 0.0263 \frac{e_o}{t^2} = 54.4 \frac{W_{max}^2}{t^2}$$

When this equation is solved for the initial tension required to give 1-percent maximum nonlinearity,

$$e_o = 2093 W_{max}^2 - 38.1t^2 \quad (5)$$

By using a maximum permissible value of strain of 0.001 inch per inch, the diaphragm design curves of figure 3 were obtained from equations (3), (4), and (5). The required initial tension, optimum maximum pressure, and optimum maximum deflection are plotted against diaphragm thickness. It will be noted that the required initial tension reaches a maximum for a thickness of about 0.002 inch (rated pressure range, 4 psi) and that no initial tension is required for thicknesses of more than 0.0067 inch (pressure range about 60 psi). Also, the curves show that a full-scale deflection of 0.0005 inch or more can be realized only for pressure ranges between about 1 pound per square inch and 200 pounds per square inch.

Figure 4 gives the pressure-deflection curves, defined by equation (3), at various values of initial tension for a gage having a diaphragm thickness of 0.004 inch (rated pressure range, 15 psi). The lines of maximum permitted strain and nonlinearity were obtained from equations (4) and (5). The intersection of these lines gives the optimum maximum pressure and deflection. Table I gives the diaphragm thickness and approximate initial tension used for each of the standard pressure ranges. It is possible to build intermediate ranges with these same diaphragms by varying the initial tension. The amount of initial tension in a diaphragm can be estimated by comparing its computed pressure-deflection curves with its measured curve of pressure against voltage output. This procedure has been of great value when the diaphragm-stretching device described subsequently is used.

Acceleration Effects

A flat diaphragm, when subject to an acceleration normal to its surface, is acted on by a force per unit area which tends to deflect the diaphragm and which is equivalent to a pressure. Since ρt is

the weight per unit area of the diaphragm, the equivalent pressure due to a normal acceleration a, is

$$p = \frac{\rho t a}{g} \tag{6}$$

From this expression it has been calculated that an acceleration of 100g normal to the diaphragm will give an error that will vary from about 3 percent of full scale for the 1-pound-per-square-inch gage to about 0.3 percent of full scale for the 100-pound-per-square-inch gage.

Because of its sturdy construction and because of its small diaphragm deflections, the gage has been found to be unaffected by very high accelerations parallel to the diaphragm. Also, it has been found that the natural frequencies of the gages are too high to be excited by the usual mechanical vibrations encountered in aeronautical work.

Diaphragm Resonance

References 2 to 8 give solutions for two types of vibrating flat circular diaphragms clamped at the boundary. One type is a plate without initial tension, and the other is an infinitely thin, perfectly flexible membrane under radial tension. Since the diaphragm of the NACA miniature pressure gage has a definite thickness relative to its diameter, it must be considered a plate under tension, the intermediate case between these two types of diaphragms. The expressions for the motions of such a stretched plate are quite involved; therefore, in order to save laborious trial-and-error calculations, it was necessary to devise a graphical solution for the natural frequencies. This solution is represented by the curve of figure 5 (see appendix for derivation and explanation) which permits a simple accurate calculation of the fundamental undamped natural frequency of any clamped circular flat diaphragm under radial tension. Similar curves could be devised for other modes of resonance, but the frequencies would be too high to be of interest in this discussion.

The fundamental natural frequencies of the $\frac{5}{16}$-inch-diameter diaphragms in the NACA miniature pressure gages were readily calculated by this method and are shown in figure 6. A curve of natural frequency against initial tension is plotted for each of the standard diaphragm thicknesses. The initial tension required in each diaphragm for 1-percent maximum nonlinearity (fig. 3) is also shown. It will be noted that the curves for the thinner diaphragms approach the one for a stretched membrane (also shown in fig. 6), and the curves for the

thicker diaphragms become nearly vertical so that their natural frequencies approach those of unstretched plates (intersections of curves and horizontal axis of fig. 6). It will also be noted that, without initial tension, the thinner diaphragms would have quite low fundamental natural frequencies.

Acoustical Resonance

Possible errors due to acoustical resonance may be avoided in the design of a dynamic pressure gage by permitting the diaphragm to be directly exposed to the pressure being measured. However, there are many instances where such a gage is not satisfactory. When pressure gradients are high, the exposed diaphragm may be too large for point measurements. Also, a flush-diaphragm-gage installation is usually more difficult and may disturb the surface contour and finish of the model. Since the diaphragm of a small gage built to measure low pressures is usually thin and fragile, it would be subject to damage if exposed. For these reasons, and in order to obtain an improved gage design as discussed previously, the pressure to be measured by the NACA miniature gage reaches the diaphragm through a small opening.

The acoustical natural frequency ω_a and damping ratio ζ of a gage having a pressure inlet leading to a cavity may be approximated by the equations, references 4 to 9, for a Helmholtz resonator (see fig. 7):

$$\omega_a = V_c\sqrt{\frac{A}{sl}} \tag{7}$$

$$\zeta = \frac{4\mu V_c}{R^3\gamma p_o}\sqrt{\frac{sl}{\pi}} \tag{8}$$

In these relations it is assumed that all dimensions, especially the inlet length, are small compared to the wave length of the resonant frequency, that the diaphragm is relatively stiff, and that the cavity volume is large compared with the inlet volume. Although these assumptions are not entirely true for the miniature gage, equation (7) does show that, for a high natural frequency, the inlet must be short and of large diameter and the cavity must be small. It will also be noted that, with fixed gage dimensions, $\omega_a \propto V_c$ and, hence, for a given gas, $\omega_a \propto \sqrt{T}$. Measured values of ω_a are approximately 30 percent lower than those obtained by using equation (7). In addition to these conditions, equation (8) is only valid for laminar flow in the inlet and this expression is also an approximation, especially when amplitudes

are high. However, it can be seen that, in addition to being dependent on absolute temperature, the damping ratio of a gage in a given gas varies inversely with the initial steady-state absolute pressure p_o. Measured values of the damping ratio of the miniature gage at standard atmospheric conditions are close to 0.1.

Over-all Frequency Response

In a typical miniature-gage installation, one side of the gage is connected through a short orifice to the pressure to be measured, and the other side, or reference side, is connected through a longer tube to a reference pressure, often atmospheric. The reference side, unless it is connected to a sharply resonant tubing system, has little effect on the over-all frequency response of the gage as is shown by the experimental results presented subsequently. Hence, excluding the reference side of the gage, the over-all frequency response is determined by two coupled resonant systems: the diaphragm and the acoustical resonant system on the measuring side of the gage. Since this coupling is low, as shown in reference 3, page 105, and since the diaphragm natural frequency is made comparatively high, the acoustical resonance is the main determining factor at the lower frequencies. Thus, to a reasonable approximation, the over-all amplitude response and phase shift up to 3000 or 4000 cycles per second is that of a single-degree-of-freedom system with viscous damping (references 2 and 3) having parameters determined by the acoustical resonance. Such a system has less than 10^o of phase shift up to approximately 60 percent of its natural frequency when its damping ratio is 0.1 or lower. Its amplitude response is flat within 5 percent up to about 23 percent of ω_a when $\zeta = 0.1$. Hence, no additional damping of the miniature gage is needed for measurements where low phase shift is desired and frequencies are reasonably low, for example, pressure distributions on an oscillating airfoil. However, where minimum distortion of a high-frequency nonsinusoidal pressure wave form is desired, the damping ratio should be adjusted to a value of approximately 0.65. This adjustment is accomplished by experimentally inserting one or more layers of closely woven silk or nylon cloth across the gage opening. With optimum damping, the amplitude response can be made flat within 5 percent up to about 70 percent of ω_a, and the phase shift increases approximately linearly to a value of 90^o at ω_a.

When the acoustical resonance of the gage itself is modified by an added length of inlet tubing, the Helmholtz resonator expression, equation (7), can still be used to approximate the lowered natural frequency, provided the total inlet length is small compared to the wave length of this frequency. If the inlet length is comparatively long, the relations using the distributed constants of the tube must be employed,

reference 10. If the added tubing is over about $\frac{1}{8}$-inch inside diameter, the gage cavity can be assumed to be negligibly small; this assumption simplifies the relations to those for a resonant tube closed at the gage end.

Electrical Features

Reference 11 gives the following relation between the change in inductance $\Delta L/L$ of a variable-air-gap type coil and the change in its air-gap length $\Delta l_2/l_2$:

$$\pm\frac{\Delta L}{L} = \mp\frac{\Delta l_2}{l_2}\left[1 - \left(\frac{l_1}{l_2\mu_o} \mp \frac{\Delta l_2}{l_2}\right) + \left(\frac{l_1}{l_2\mu_o} \mp \frac{\Delta l_2}{l_2}\right)^2 - \cdots\right] \tag{9}$$

The inductances of the two coils of the miniature gage change simultaneously, one increasing, and one decreasing, and it is shown subsequently that the gage output is proportional to the sum of these two changes of inductance. From equation (9) this sum is approximately:

$$2\,\frac{\Delta l_2}{l_2}\left[1 - \frac{l_1}{l_2\mu_o} + \left(\frac{l_1}{l_2\mu_o}\right)^2 + \left(\frac{\Delta l_2}{l_2}\right)^2\right] \tag{10}$$

Since expressions (9) and (10) are based on an ideal toroidal coil having no magnetic-flux leakage, they are not exact for the miniature gage. However, they do show that the use of two push-pull coils considerably increases the linear range of a gage. A value of 0.010 inch was chosen for the length of the air gaps in the miniature gages. This length was found to give a reasonable output and at the same time permitted accurate matching of the two air gaps with usual machine-shop tolerances. If the diaphragm deflection is assumed to vary linearly with pressure, expression (10) indicates that the output of a typical miniature gage having an air-gap change of 5 percent would be about 1/4 percent nonlinear. A similar single-air-gap gage would be about 5 percent nonlinear. Expressions (9) and (10) also show that, for maximum output and for minimum effects of any variations in the magnetic qualities, the gage should be made of a material having a high initial permeability (see fig. 2) so that the term $l_1/l_2\mu_o$ will be small compared with unity. The value of this term for the miniature gage is quite small, approximately 0.01 when a value of 4200 is assumed for the initial permeability of the 42-percent nickel alloy.

Since it was not practical to laminate the core structure of the miniature-gage coils, their effective resistance is appreciably increased at the higher carrier frequencies owing to eddy-current losses. The expressions for this increased resistance are rather involved, but it can be shown, reference 11, that it varies with air-gap length in a manner somewhat similar to that already described for an inductance.

Most of the bridge circuits in which the miniature gage is used can be represented by the simplified circuit of figure 8 with reasonable accuracy. It has been assumed that, with no pressure applied to the gage, the impedance of each coil Z is the same and that the resistance of each of the other bridge arms R is the same. When a differential pressure is applied to the gage, the impedance of one coil increases an amount ΔZ_1 while the impedance of the other coil decreases an amount ΔZ_2. In each case the impedance changes are due to the vector sum of an inductance change and a resistance change, each of which is assumed to be linear with pressure changes. The voltage output V_o of such a bridge, references 11 to 13, is given by the following relation:

$$V_o = \frac{\Delta Z_1 + \Delta Z_2}{2Z} \frac{R_L}{2R_L + R + Z} V_i \tag{11}$$

For the small air-gap changes of the miniature gage, $\Delta Z_1 \approx \Delta Z_2 \approx \Delta Z$. When the load resistance R_L is high compared with the bridge impedance, $\frac{R_L}{2R_L + R + Z} \approx \frac{1}{2}$. With these approximations, equation (11) becomes:

$$V_o = \frac{\Delta Z}{Z} \frac{V_i}{2} \tag{12}$$

If the following relations be defined,

$$Z = R_e + j\omega L \qquad Q = \frac{\omega L}{R_e}$$

$$\Delta Z = \Delta R_e + j\omega \Delta L \qquad \Delta Q = \frac{\omega \Delta L}{\Delta R_e}$$

then equation (12) can be expressed in polar form as follows:

$$V_o = \frac{\Delta L}{L} \frac{Q}{\sqrt{1 + Q^2}} \frac{\sqrt{1 + (\Delta Q)^2}}{\Delta Q} \frac{V_i}{2} \angle \left(\tan^{-1}\Delta Q - \tan^{-1}Q\right) \tag{13}$$

where the angle gives the phase relation between the input and output voltages. When ΔR_e is negligibly small, ΔQ is large, $\frac{\sqrt{1 + (\Delta Q)^2}}{\Delta Q} \approx 1$, and equation (13) reduces to:

$$V_o = \frac{\Delta L}{L} \frac{Q}{\sqrt{1 + Q^2}} \frac{V_i}{2} \angle \tan^{-1}\left(\frac{1}{Q}\right) \qquad (14)$$

Equations (13) and (14) show that for maximum output the Q of the coils should be high so that $Q/\sqrt{1 + Q^2}$ approaches unity. At the same time the coils should permit the use of a reasonably high input voltage V_i without overheating and without drawing excessive power from the carrier oscillator. The coils should be wound with a material having a low temperature coefficient of resistance, and the wire size should be large enough to be conveniently handled. In addition, most carrier systems are built to match gages having an impedance of several hundred ohms. With the severe space limitations in the miniature gage, these conflicting requirements were difficult to meet. However, coils wound with 150 turns of B. & S. No. 38 manganin wire were found to give a reasonable output over a wide range of carrier frequencies in spite of their low values of Q. Figure 9 gives the inductance L and effective resistance R_e of a typical miniature-gage coil with 4 feet of vinyl-covered cable attached as measured at various frequencies with an Anderson type impedance bridge (references 12 to 14). The percentage change in these properties due to full-scale pressure was measured at the same time, and the terms $(\Delta L/L)_{max}$, $(\Delta R_e/R_e)_{max}$, and $(\Delta L/L)_{max}\left(Q/\sqrt{1 + Q^2}\right)\left(\sqrt{1 + (\Delta Q)^2}/\Delta Q\right)$ are also plotted against frequency in figure 9.

Associated Carrier Equipment

Figure 10 gives a block diagram of the carrier equipment normally used with inductance-type gages. The bridge output is amplified, demodulated, and applied to the recorder as a current proportional to the magnitude and direction of the gage pressure. Since an iron-core gage will generally produce third harmonics of its input frequency, the third-harmonic filter is necessary if full input voltage is applied to the gage and a high-gain amplifier is used. The phase-shift circuit compensates for any phase shift in the bridge circuit or amplifier, so that maximum gage sensitivity may be obtained.

Carrier systems as outlined in figure 10 and with oscillator frequencies of 3 to 25 kilocycles per second have been successfully used with the miniature gages. In order to supplement commercially available carrier equipment built to drive recording galvanometers up to about 500 cycles per second, two additional systems have been built at the Langley Laboratory especially for the miniature gages. One system, built to utilize the high-frequency response of the miniature gages, has a 25-kilocycle-per-second oscillator and an output circuit designed to drive a cathode-ray oscilloscope. Another system, built as simply as possible in units having up to 18 channels, is used to drive very sensitive galvanometers when the pressure frequencies are expected to be below about 100 cycles per second. As shown in the typical circuit of figure 11, the gage output is demodulated directly, and the amplifier, filters, and phase-shift circuit of figure 10 are omitted. A 10-kilocycle-per-second oscillator is used and, when necessary, the germanium crystals are put in a small temperature-controlled oven for increased stability.

CONSTRUCTION DETAILS

Photographs of the two most widely used models of the miniature pressure gage are shown in figure 12. They differ only in their external features. Model 49-NC is built for general use and is characterized by a cable clamp and pressure nipples used to facilitate both mounting and making pressure connections. In the model 49-TP gage, built for minimum thickness, the pressure nipples are omitted and the pressure openings are No. 2-64 N. F. tapped holes. The cable clamp is also omitted, and the electrical connections are protected by filling the space between the small flanges with either a hard wax or Paraplex, a catalytic setting plastic. Another smaller group of gages, built to be installed in a series of small oscillating models, have nipples on one side and tapped pressure openings on the other side. Several gages, built for installations where a minimum diameter is required, have no flanges at the cable connections, and the lead-in pins make a sharp bend near the gage.

Detailed drawings for the model 49-NC gage are given in figures 1 and 13 and are largely self-explanatory. Other models have the same basic dimensions. Excluding pressure and electrical connections, all of the gages are 7/16 inch in outside diameter, 1/4 inch thick, and their diaphragms have an active diameter of 5/16 inch. The two case halves of each gage are paired so that the 0.010-inch-air-gap dimensions agree within 0.0005 inch. All the coils are wound so that the number of turns (150) match within one turn, and the two coils for a gage are selected so that the direct-current resistances match within 1 ohm. The Glyptal, used to cement the coils in place and to pressure-seal the joints around the lead-in wires, has been found to be little affected by the soldering heat, provided it is properly baked in place.

The soldering jig shown in figure 14 is used when soldering the diaphragm in place. This jig is made of type 303 stainless steel which has a thermal coefficient of expansion approximately three times that of the 42-percent nickel alloy. A piece of diaphragm material 1 inch in diameter is clamped in the jig at room temperature. (The size of the jig is limited because the thinner diaphragm material is available only in widths of 1 in. or less.) A pair of case halves with the coils cemented in place is mounted in the jig as shown. In order to stretch the diaphragm material, the entire assembly is then heated in an oven to a temperature between 100° F and 175° F above room temperature, depending on the initial diaphragm tension required for the particular pressure range. The exact jig temperature is also determined by variations in the gage material and in the subsequent soldering techniques. When the jig has reached the correct temperature, it is removed from the oven and the diaphragm is soldered to the case halves with a small jewelers alcohol torch. Although the temperature of the heavy jig will not change rapidly, much care must be exercised during the soldering operation to obtain repeatable temperature gradients in the various parts if the initial diaphragm tension is to be controlled.

Although construction of consistently satisfactory miniature gages is not simple, it can be accomplished by reasonably experienced instrument technicians. The 42-percent nickel alloy, like most high-nickel steels, requires special machining techniques because of its toughness and tendency to "bug" the tools. The small coils are tedious to wind, and experience is required to obtain the proper initial tension consistently when soldering the diaphragms. However, the gage is composed of only a few parts of simple shape and, whether it was made at the Langley Laboratory or under contract, construction costs have proved to be somewhat less than the cost to NACA of other available electrical gages used to record fluctuating pressures.

Some typical gage installations are illustrated by the sketches of figure 15. In each case shown the pressure orifice may be drilled, and the surface on which the pressure is to be measured may be finished before the gage is installed. If it is desired to measure the difference between the upper- and lower-surface pressures on the small solid airfoil of figure 15(c), the airfoil may be split and the gages clamped between the two halves as in the cone of figure 15(d). If splitting the airfoil is impractical, the gages are usually installed as in figure 15(c) except that short lengths of thick-wall tubing connect the lower side of the gages to the lower surface. In this case the orifices are usually tapped for small plugs (often No. 0-72) to prevent entry of foreign particles while the surface is being finished.

PERFORMANCE TESTS

Output

The full-scale open-circuit output of a 15-pound-per-square-inch miniature pressure gage at various carrier frequencies is given by the curve of figure 16. The bridge circuit used, shown in figure 17, is incorporated in many carrier systems. The outputs of other ranges of the gage vary with frequency in the same manner. Average values of the full-scale output of each of the standard pressure ranges, when used with the bridge circuit of figure 17 at 10 kilocycles per second, are given in table I.

Figure 18 gives a calibration curve of current output against pressure obtained when a 4-pound-per-square-inch gage was used with 3000-cycle-per-second carrier equipment, Consolidated Engineering Corp. System D. Refer to figure 10 for a block diagram of the equipment. A medium gain setting of the amplifier was used. With this carrier equipment, about 1/10 of the full-scale gage pressure gave full-scale output when the amplifier gain setting was a maximum.

Linearity

An expanded plot of the typical calibration curve of figure 18 showed that its maximum deviation from its straight-line portion is approximately 2 percent of full scale. Further tests revealed that about one-half of this deviation was caused by the carrier equipment, so that the maximum nonlinearity of the gage was about 1 percent. This value is typical of most of the miniature gages. However, gages having various amounts of maximum nonlinearity, from an imperceptible amount up to 2 percent, have been built and found to be satisfactory. Since the less-linear gages have more output, and since their nonlinearity reaches its maximum at full-scale pressure (see fig. 4), these gages are used where the pressures to be measured are expected to be somewhat less than full scale.

Hysteresis

An expanded plot of the typical calibration curve of figure 18 showed the gage to have a maximum hysteresis error of 0.7 percent of full scale. Similar tests of other miniature gages showed that their hysteresis errors are usually less than 1 percent of full scale. In other tests in which the maximum pressure applied was less than full scale, it was found that the hysteresis errors were correspondingly smaller.

Temperature Effects

Over the temperature range of -50° F to 200° F, the shift in gage output due to temperature changes (zero drift) has been found to be less than 0.02 percent of full scale per degree for most of the gages tested. Over the same range, tests have shown that the change in sensitivity with temperature is usually less than 0.03 percent of full scale per degree. However, it has not always been possible to obtain well-matched diaphragm and case materials, and changes of sensitivity with temperature up to 0.2 percent of full scale per degree were noted for one lot of gages. The temperature errors are consistent and may be corrected if the approximate gage operating temperature is known.

Acceleration Effects

A typical 8-pound-per-square-inch gage was mounted on a laboratory horizontal vibrating table so that accelerations acted normal to the diaphragm. Accelerations up to 22g at frequencies up to 60 cycles per second were applied. The resulting outputs were recorded with auxiliary equipment as outlined in figure 10 and were compared with a pressure calibration of the gage. The output due to the acceleration forces was found to be 0.013 percent of full-scale output per g. This value and the results of other similar tests agree reasonably well with values computed by means of equation (6).

In order to check gage operation when subject to high accelerations parallel to the diaphragm, calibrations were made while the gage was mounted on a spinning disk. Electrical connections from the gage were brought out through specially treated slip rings and the pressure connection through a rotating pressure seal. Two series of tests were made, one up to 2100g with the gage mechanically clamped and another up to 4400g with the gage embedded in Wood's metal. No measurable zero drift or sensitivity change was observed. The accuracy of measurement was limited by the slip rings to 2 percent of full scale for zero drift and 1/2 percent of full scale for sensitivity change. Miniature gages have also been embedded in Wood's metal and mounted on other rotating devices where the computed acceleration, acting approximately parallel to the diaphragm, was as high as 28,000g. Although no calibrations were made while the gages were being rotated, the gages were found to be undamaged when later tested.

Amplitude Response and Phase Shift

Records were made of the miniature-gage output when the lower resonant frequencies were pulse-excited. A direct-current bridge circuit

and a recording oscilloscope were used. Although this method produced an output proportional to the rate of change of the pressure, the resonant frequency and the rate at which it was damped were unchanged. The acoustical damped free resonant frequency was excited by rapidly passing a small jet of air across the pressure inlet. From such tests (made in air at normal room conditions), the acoustical natural frequency was found to average about 4200 cycles per second for the model 49-NC gage and about 5800 cycles per second for the model 49-TP gage. The damping ratio in each case was found to be approximately 0.1. Records of diaphragm resonant frequencies, excited by striking the gage case with a small metallic object, gave natural frequencies that agreed with those predicted in figure 6 within the accuracy with which the initial tension could be estimated, about 10 percent.

The pressure pulsator shown in figure 19 was built at the Langley Laboratory to check the frequency response of dynamic-pressure gages, actual installation conditions being simulated where practical. The motor-driven sine-wave cam rotating past the rectangular air jet causes the pressure to vary approximately sinusoidally at the gage location. Pressure pulsations from 25 to 3000 cycles per second with amplitudes up to 1 pound per square inch peak-to-peak can be reliably obtained. A piezoelectric pressure gage (manufactured by Massa Laboratories, Inc.) is used as a standard. The pulsator is frequently run in an altitude chamber to control pressure and temperature which govern the acoustical characteristics as was shown in the section entitled "Acoustical Resonance."

By means of this pulsator and the 25-kilocycle-per-second carrier equipment, calibration curves of frequency against amplitude response were made in air at normal room conditions of a typical 8-pound-per-square-inch model 49-NC gage with no added tubing and are shown in figure 20. In order to check the effects of reference pressure connections, tests were made with the reference side (1) open and free to resonate, (2) plugged, and (3) attached to 10 feet of $\frac{1}{16}$-inch-inside-diameter tubing. These effects are seen to be small. From records of the pulse-excited resonant frequencies of this gage, the acoustical natural frequency f_a was found to be 4100 cycles per second, and the corresponding damping ratio ζ, to be 0.11. The theoretical amplitude response of a single-degree-of-freedom system having these parameter values is shown as a solid curve in figure 20. The deviations near 2000 cycles per second can be attributed to the fairly high second-harmonic content of the pulsator wave form.

The phase-shift calibration of the same gage is also shown in figure 20. Accurate measurements were difficult because of the imperfect pulsator wave form and were very unreliable above 1000 cycles per second.

However, the measured values have the same order of magnitude as the computed theoretical ones shown in the same figure.

DESIGN VARIATIONS

In addition to the $\frac{7}{16}$-inch-diameter miniature gage described in this paper, several smaller variable-air-gap pressure gages have been built at the Langley Laboratory in small quantities for special applications. One of them, model 51, is essentially the model 49 gage reduced in size. Its outside diameter is 3/16 inch, its thickness is 0.160 inch, and its diaphragm has an active diameter of 0.120 inch. It was built for applications where the regular miniature gage has been found to be too large, for example, measurements of fluctuating pressures nearer to the tip of the conical supersonic survey probe of figure 15(d).

Another design variation, model 50, is the $\frac{3}{16}$-inch-outside-diameter by $\frac{3}{4}$-inch-long flush-diaphragm gage built for shock-tube measurements and so forth. The free diaphragm diameter is also 0.120 inch, and its lowest natural frequency is 30,000 cycles per second or higher depending on the pressure range. The diaphragm is soldered on one end of the gage, and the electrical leads and the reference pressure connection are brought out of the opposite end. There is only one active coil, but a dummy coil in the gage permits the use of standard bridge circuits. The dummy coil has a silver shim instead of an air gap, and reasonable temperature compensation can be obtained by varying the thickness of the shim.

CONCLUDING REMARKS

The miniature electrical pressure gage described in this paper has proved to be of value for many types of pressure measurements in aeronautical research at the Langley Laboratory. The outstanding characteristics of the gage may be summarized as follows:

1. The gage, exclusive of pressure and electrical connections, is 7/16 inch in diameter and 1/4 inch thick.

2. The frequency response of the gage alone is approximately that of a single-degree-of-freedom system having a natural frequency of

4000 cycles per second or higher and a damping ratio of about 0.1. When the gage is installed within 1/4 inch of the point at which the pressure is to be measured, the lowest natural frequency is usually above 2500 cycles per second, and the damping can be varied to suit the type of measurement.

3. The effect of accelerating forces normal to the diaphragm is of the order of 1 percent of full scale per 100g. Accelerations of 5000g or higher parallel to the diaphragm have negligible effect.

4. Temperature errors in the range of -50° F to 200° F are normally less than 0.03 percent of full scale per degree and may be corrected.

5. Over-all accuracy when measuring steady-state or low-frequency pressures is usually limited by hysteresis errors, which are normally less than 1 percent of full scale. Measurements can be made up to 3000 cycles per second with errors of less than 5 percent with properly designed pressure inlets.

6. Gages with pressure ranges of ±0.5, ±1, ±2, ±4, ±8, ±15, ±30, ±60, and ±100 pounds per square inch have been successfully built.

7. The internal impedance of the gage is of the order of 200 ohms, and lead wires up to several hundred feet may be used between the gage and its associated equipment.

8. The output is sufficient to permit the gage to be used conveniently with carrier amplifier equipment of standard design.

9. The sturdy construction of the gage permits its use in a variety of applications without damage.

10. Construction costs compare favorably with those of other available electrical pressure gages used to record fluctuating pressures.

Langley Aeronautical Laboratory
National Advisory Committee for Aeronautics
Langley Field, Va., November 21, 1951

APPENDIX

GRAPHICAL SOLUTION FOR THE FUNDAMENTAL NATURAL FREQUENCY OF A STRETCHED, CIRCULAR, CLAMPED, FLAT DIAPHRAGM

If the assumptions are made that the diaphragm is perfectly clamped and in a vacuum, and that its deflections during vibration are relatively small, reference 8 gives the following expression for the deflection w, at any radius r, as a solution for the differential equation of motion for a circular, clamped, flat diaphragm under uniform radial tension:

$$w = \frac{p}{\omega^2 \rho t}\left[\frac{k_2 I_1(k_2R)J_0(k_1r) + k_1 J_1(k_1R)I_0(k_2r)}{k_2 I_1(k_2R)J_0(k_1R) + k_1 J_1(k_1R)I_0(k_2R)} - 1\right] \tag{A1}$$

where J_0 and J_1 are Bessel functions of the zeroeth and first order, respectively, I_0 and I_1 are Bessel functions with imaginary arguments of the zeroeth and first order, respectively, and

$$k_1 = \sqrt{\frac{\sqrt{d^2 + 4\omega^2 c} - d}{2c}}$$

$$k_2 = \sqrt{\frac{\sqrt{d^2 + 4\omega^2 c} + d}{2c}}$$

$$c = \frac{Et^2 g}{12\rho(1 - \sigma^2)}$$

$$d = \frac{Ee_0 g}{\rho}$$

At an undamped natural frequency ω_m, the deflection of a portion of the diaphragm theoretically becomes infinite, and hence from equation (A1),

$$k_2 I_1(k_2R)J_0(k_1R) + k_1 J_1(k_1R)I_0(k_2R) = 0$$

If $x = k_1R$ and $y = k_2R$ and the terms are rearranged,

$$\frac{I_0(y)}{yI_1(y)} = -\frac{J_0(x)}{xJ_1(x)} \tag{A2}$$

Figure 21 shows a plot of $-J_0(x)/xJ_1(x)$ against x and two plots of $I_0(y)/yI_1(y)$ against y, one where the horizontal scale is such that $x = y$ and one where $x = 0.1y$. The intersections of the curves give the values of x and y which satisfy equation (A2) for the particular cases where $\frac{x}{y} = 1$ and $\frac{x}{y} = 0.1$.

It will be noted that when $d = 0$ (plate without tension),

$$\frac{x}{y} = \sqrt{\frac{\sqrt{d^2 + 4c\omega_m^2} - d}{\sqrt{d^2 + 4c\omega_m^2} + d}} = 1$$

and that, when $c = 0$ (infinitely thin membrane), $\frac{x}{y} = 0$. Since only positive values of c, d, and ω_m are practical, there are no values of interest of x/y except between these limits. Hence, it can be seen from figure 21 that, at the first or fundamental natural frequency, x is limited in value to the range from $x = 2.405$ $\left(\frac{x}{y} = 0 \text{ and } y = \infty\right)$ to $x = y = 3.196$. Table II gives corresponding values of x and y obtained from expanded plots of $-J_0(x)/xJ_1(x)$ against x and $I_0(y)/yI_1(y)$ against y for various values of x/y in this range.

Further simplification is necessary to permit a straightforward method of calculating natural frequencies. From the preceding definitions,

$$x = k_1R = R\sqrt{\frac{\sqrt{d^2 + 4\omega_m^2 c} - d}{2c}}$$

$$y = k_2R = R\sqrt{\frac{\sqrt{d^2 + 4\omega_m^2 c} + d}{2c}}$$

hence

$$x^2 = \frac{R^2}{2c}\left(\sqrt{d^2 + 4\omega_m{}^2 c} - d\right)$$

$$y^2 = \frac{R^2}{2c}\left(\sqrt{d^2 + 4\omega_m{}^2 c} + d\right)$$

and

$$y^2 - x^2 = \frac{R^2 d}{c} \tag{A3}$$

Also

$$x^2 y^2 = \frac{R^4 \omega_m{}^2}{c}$$

and hence

$$xy = \frac{R^2 \omega_m}{\sqrt{c}} \tag{A4}$$

Substituting the previously defined values of c and d into equations (A3) and (A4) yields

$$y^2 - x^2 = \frac{12R^2 e_o(1 - \sigma^2)}{t^2} \tag{A5}$$

$$xy = \frac{2R^2 \omega_m \sqrt{3\rho(1 - \sigma^2)}}{t\sqrt{Eg}} \tag{A6}$$

The corresponding values for these two expressions are also tabulated in table II. Figure 5 shows a plot of $2R^2\omega_m\sqrt{3\rho(1 - \sigma^2)}\Big/t\sqrt{Eg}$ against $12R^2 e_o(1 - \sigma^2)\Big/t^2$ throughout the range needed for the miniature-gage diaphragm calculations. This solution can be used to compute the fundamental natural frequency of any circular, clamped, flat diaphragm under radial tension. With the same procedure, a similar curve could be plotted for other modes of resonance.

To use this graphical method, it is merely necessary to:

(1) Calculate $12R^2e_o(1 - \sigma^2)/t^2$ from the initial tension (expressed as strain) and the diaphragm constants

(2) With the value obtained in step (1), obtain the value of $2R^2\omega_m\sqrt{3\rho(1 - \sigma^2)}/t\sqrt{Eg}$ from the graphical solution

(3) Calculate $2R^2\sqrt{3\rho(1 - \sigma^2)}/t\sqrt{Eg}$

(4) Divide the value obtained in step (2) by the value obtained in step (3) to obtain the natural frequency

REFERENCES

1. Griffith, A. A.: The Theory of Pressure Capsules. Part I.- General Discussion. Part II.- The Complete Flat Disc without Control Spring. R. & M. No. 1136, British A.R.C., 1927.

2. Timoshenko, Stephen: Vibration Problems in Engineering. Second ed., D. Van Nostrand Co., Inc., 1937.

3. Den Hartog, J. P.: Mechanical Vibrations. Third ed., McGraw-Hill Book Co., Inc., 1947.

4. Rayleigh, (Lord): The Theory of Sound. Second ed., Macmillan & Co., Ltd. (London), 1896. (Reprinted 1929.)

5. Lamb, Horace: The Dynamical Theory of Sound. Second ed., Edward Arnold & Co. (London), 1931.

6. Morse, Philip M.: Vibration and Sound. First ed., McGraw-Hill Book Co., Inc., 1936.

7. Crandall, Irving B.: Theory of Vibrating Systems and Sound. D. Van Nostrand Co., Inc., 1926.

8. Mason, Warren P.: Electromechanical Transducers and Wave Filters. D. Van Nostrand Co., Inc., 1942.

9. Delio, Gene J., Schwent, Glennon V., and Cesaro, Richard S.: Transient Behavior of Lumped-Constant Systems for Sensing Gas Pressures. NACA TN 1988, 1949.

10. Taback, Israel: The Response of Pressure Measuring Systems to Oscillating Pressures. NACA TN 1819, 1949.

11. Neubert, H. K. P.: Design and Performance of Inductance Pick-Ups and Their Associated Circuits. Rep. No. Instn. 7, British R.A.E., Sept. 1948.

12. Laws, Frank A.: Electrical Measurements. Second ed., McGraw-Hill Book Co., Inc., 1938.

13. Hague, B.: Alternating Current Bridge Methods. Fourth ed., Sir Isaac Pitman & Sons, Ltd. (London), 1938.

14. Smith, Arthur Whitmore: Electrical Measurements in Theory and Application. Third ed., McGraw-Hill Book Co., Inc., 1934.

TABLE I

THE STANDARD PRESSURE RANGES OF THE NACA MINIATURE GAGE

AND SOME OF THEIR CHARACTERISTICS

Standard pressure range (psi)	Diaphragm thickness, t (in.)	Approximate initial tension, e_o (in./in.)	Average full-scale output (mv) (a)
0.5	0.001	0.00025	30
1	.001	.0004	35
2	.0015	.0005	40
4	.002	.0005	45
8	.003	.0005	52
15	.004(B. & S. 38)	.00035	60
30	.0056(B. & S. 35)	.00015	65
60	.0071(B. & S. 33)	0	70
100	.0089(B. & S. 31)	0	55

[a]As measured with the bridge circuit of figure 17 with an input voltage of 10 volts at 10 kilocycles per second.

TABLE II

TABULATED VALUES OF THE GRAPHICAL SOLUTION FOR THE FUNDAMENTAL UNDAMPED NATURAL FREQUENCY OF ANY CIRCULAR, CLAMPED, FLAT DIAPHRAGM UNDER RADIAL TENSION

x/y	x	y	$\frac{xy}{2R^2\omega_m\sqrt{3\rho(1-\sigma^2)}/t\sqrt{Eg}}$	$\frac{y^2-x^2}{12R^2e_o(1-\sigma^2)/t^2}$
[a]1.0	3.1962	3.1962	10.22	0
.95	3.170	3.337	10.58	1.086
.9	3.143	3.492	10.98	2.317
.85	3.114	3.664	11.41	3.725
.8	3.083	3.854	11.88	5.347
.75	3.051	4.068	12.41	7.240
.7	3.018	4.311	13.01	9.480
.65	2.983	4.589	13.69	12.16
.6	2.947	4.912	14.48	15.44
.55	2.909	5.281	15.36	19.43
.5	2.869	5.738	16.46	24.69
.45	2.828	6.284	17.77	31.50
.4	2.786	6.965	19.40	40.75
.35	2.742	7.834	21.48	53.86
.3	2.696	8.987	24.23	73.49
.25	2.649	10.60	28.07	105.3
.2	2.602	13.01	33.85	162.5
.15	2.553	17.02	43.45	283.2
.1	2.505	25.05	62.75	621.2
.075	2.480	33.07	82.01	1087.3
.05	2.455	49.10	120.5	2405
.025	2.430	97.20	236.2	9442
[b]0	2.4048	∞	∞	∞

[a]Plate without tension.

[b]Infinitely thin membrane.

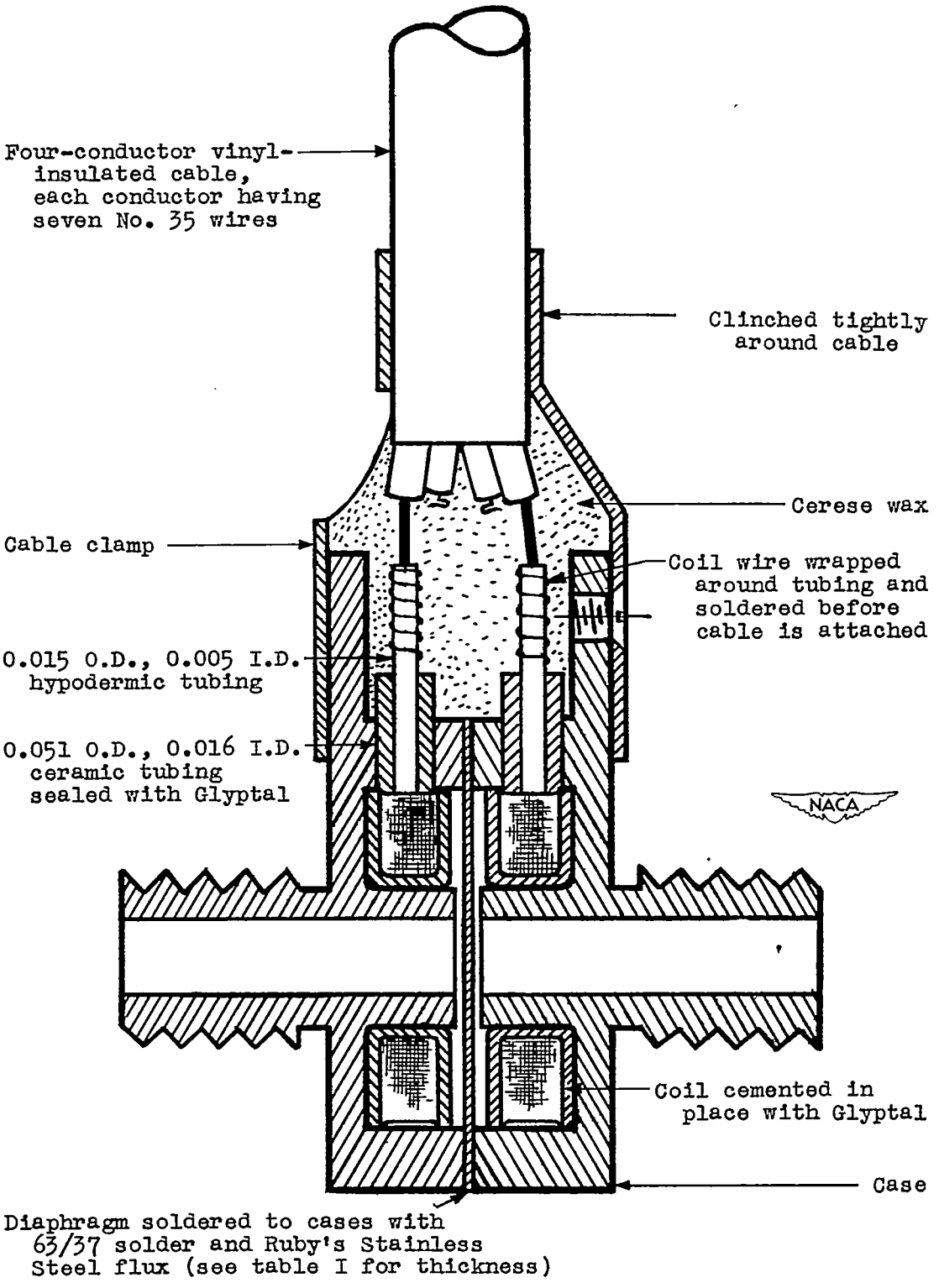

Figure 1.- Sectional view of NACA miniature electrical pressure gage model 49-NC.

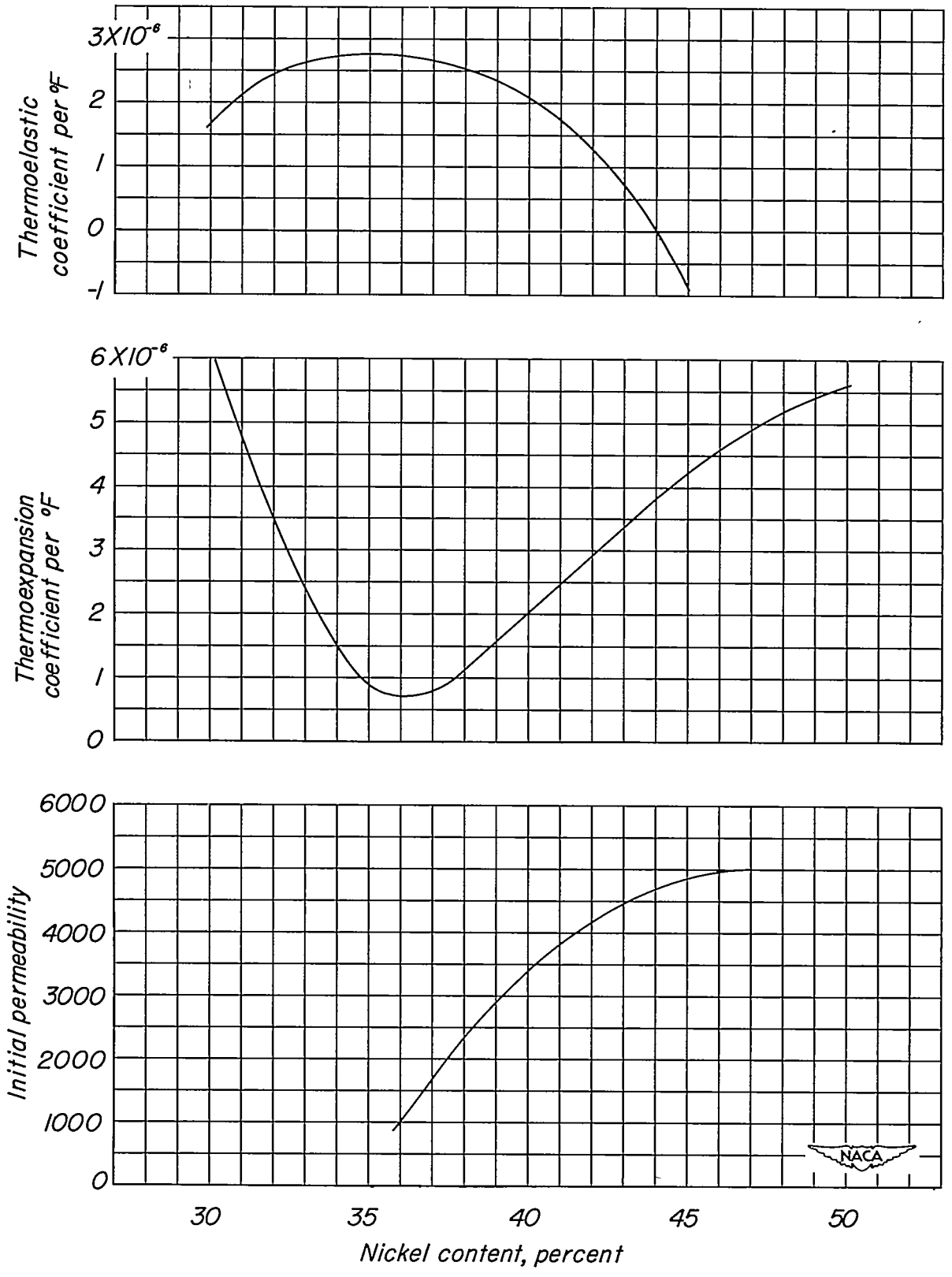

Figure 2.- Some properties of nickel-iron alloys.

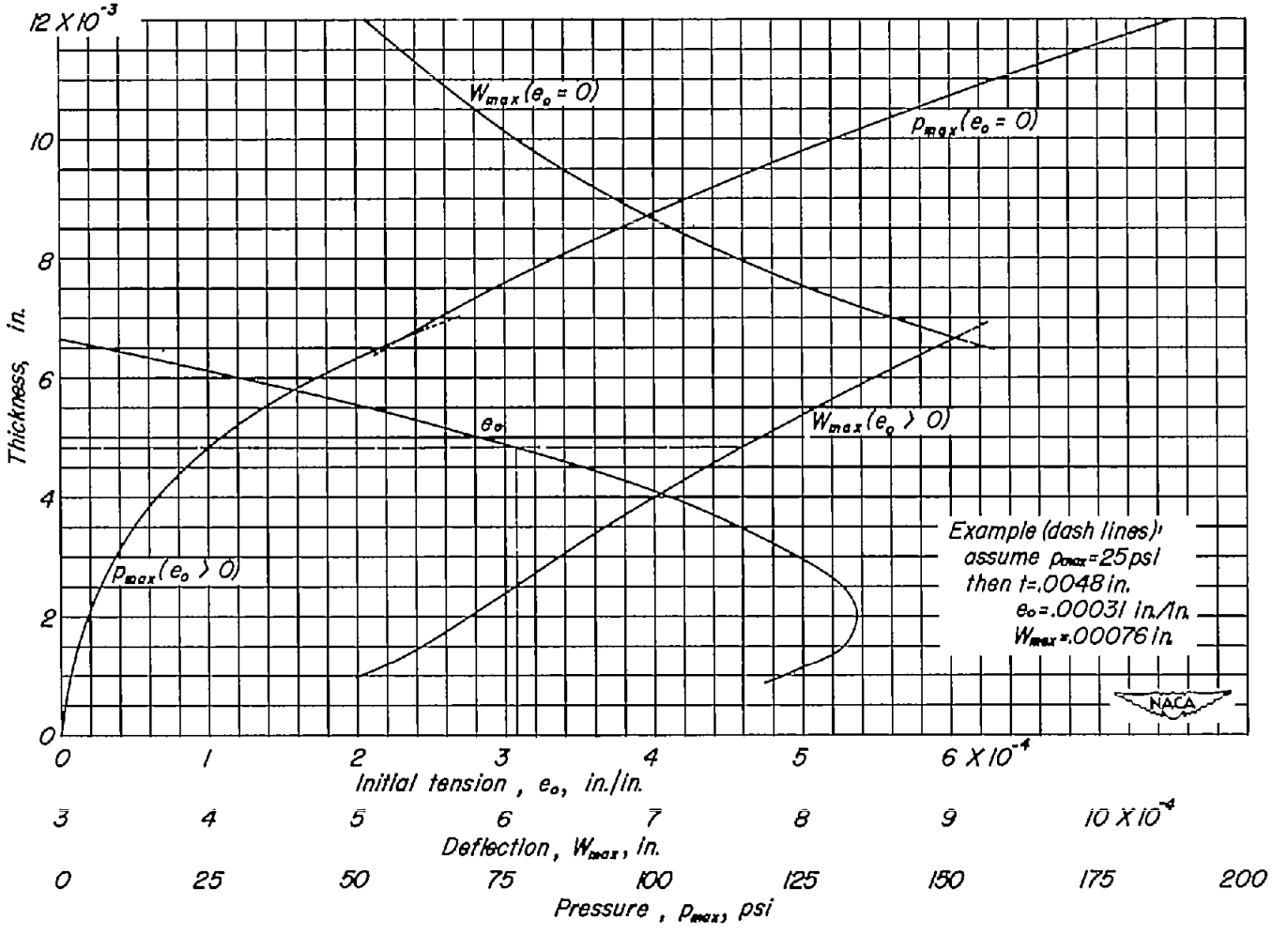

Figure 3.- Design curves for $\frac{5}{16}$-inch-diameter, 42-percent-nickel-alloy, flat, stretched diaphragms. Maximum allowed strain, 0.001 inch per inch; maximum allowed nonlinearity, 1.0 percent.

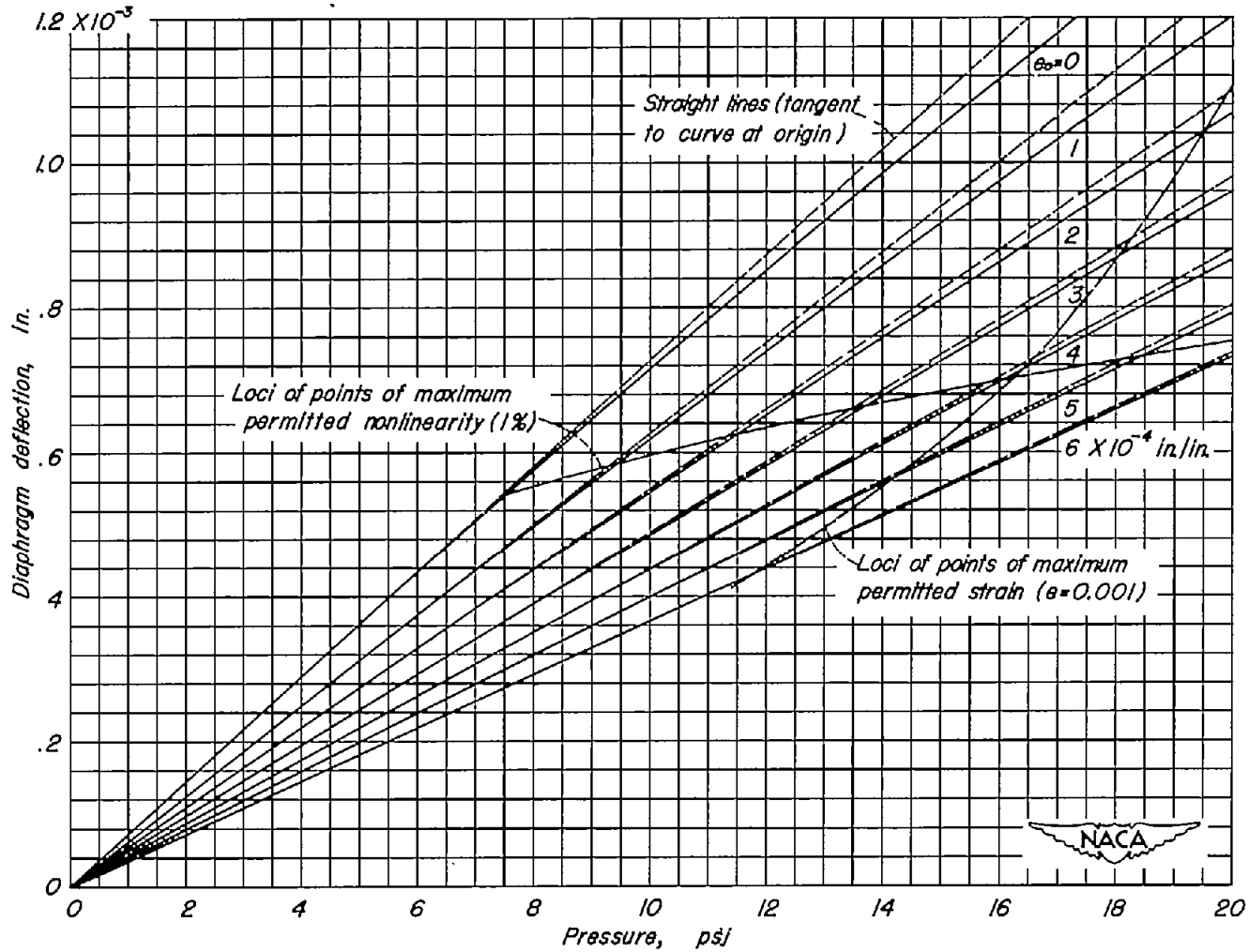

Figure 4.- Curves of deflection against pressure for a typical diaphragm of an NACA miniature electrical pressure gage. Rated pressure range, 15 pounds per square inch; diaphragm thickness, t = 0.004 inch.

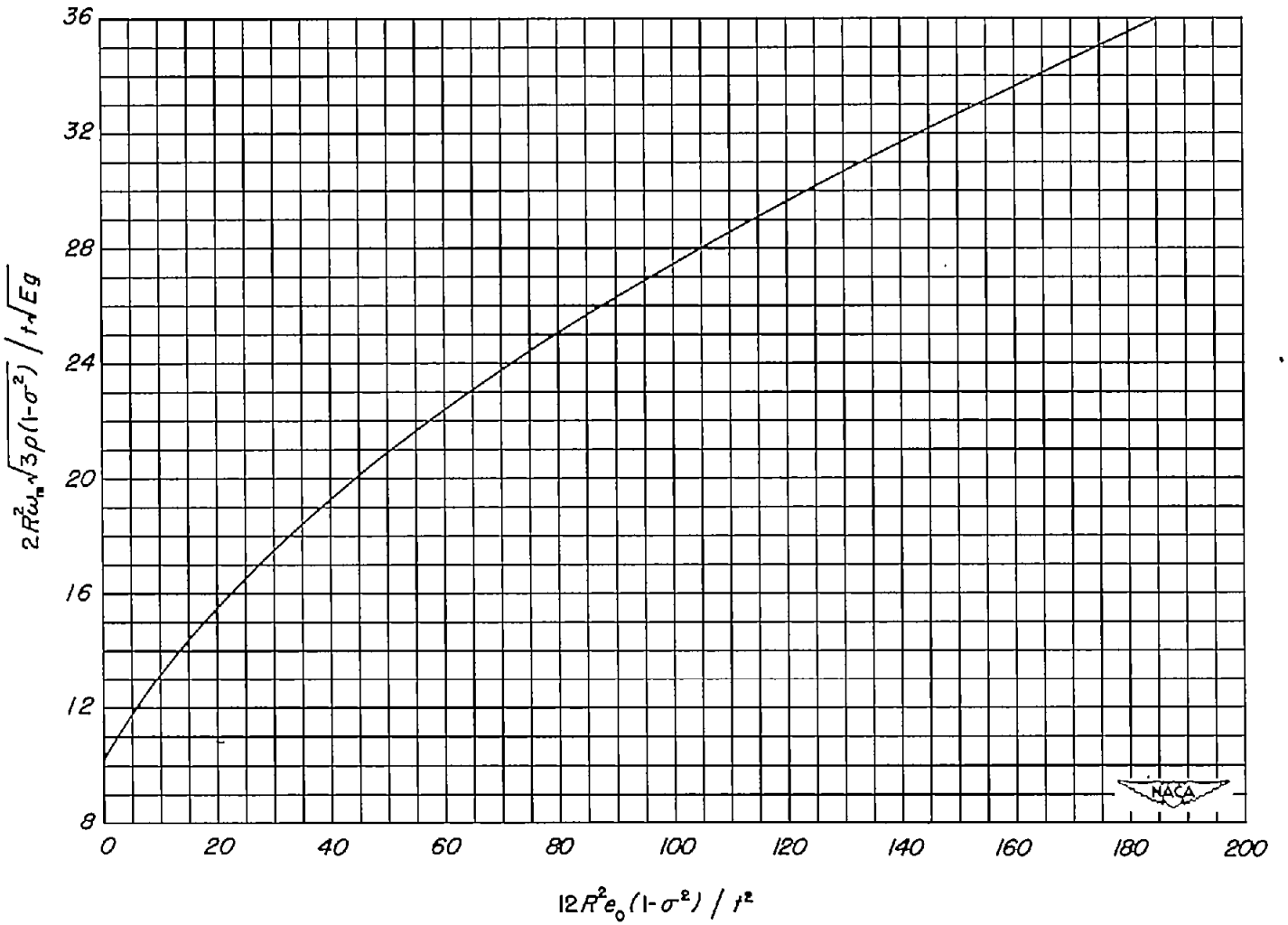

Figure 5.- Graphical solution for the fundamental natural frequency of any clamped, circular, flat diaphragm under radial tension.

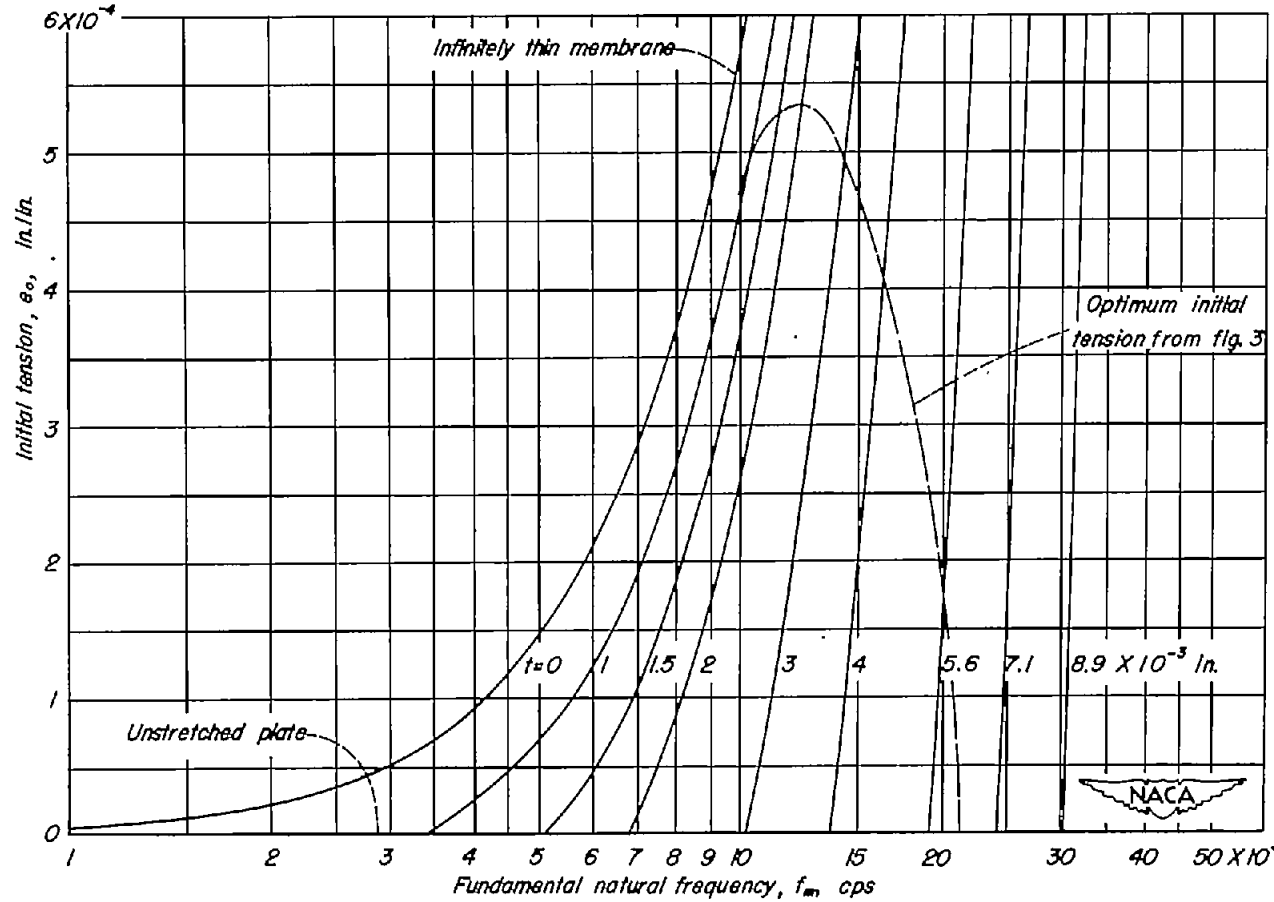

Figure 6.- Computed fundamental natural frequencies of diaphragms of the NACA miniature electrical pressure gage.

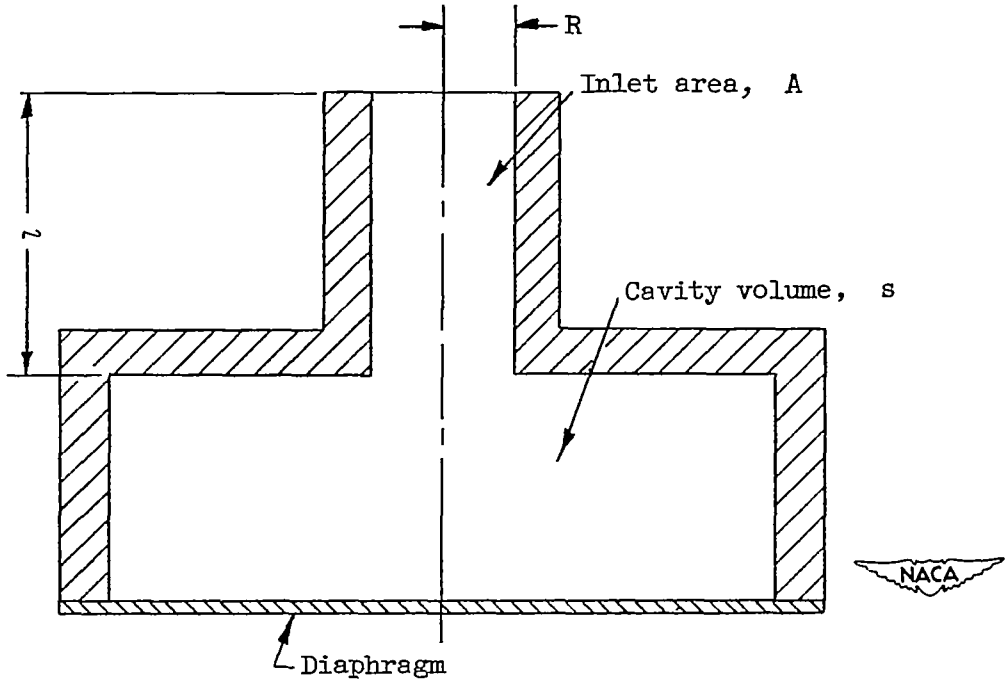

Figure 7.- Sketch of Helmholtz resonator showing symbols used in this paper.

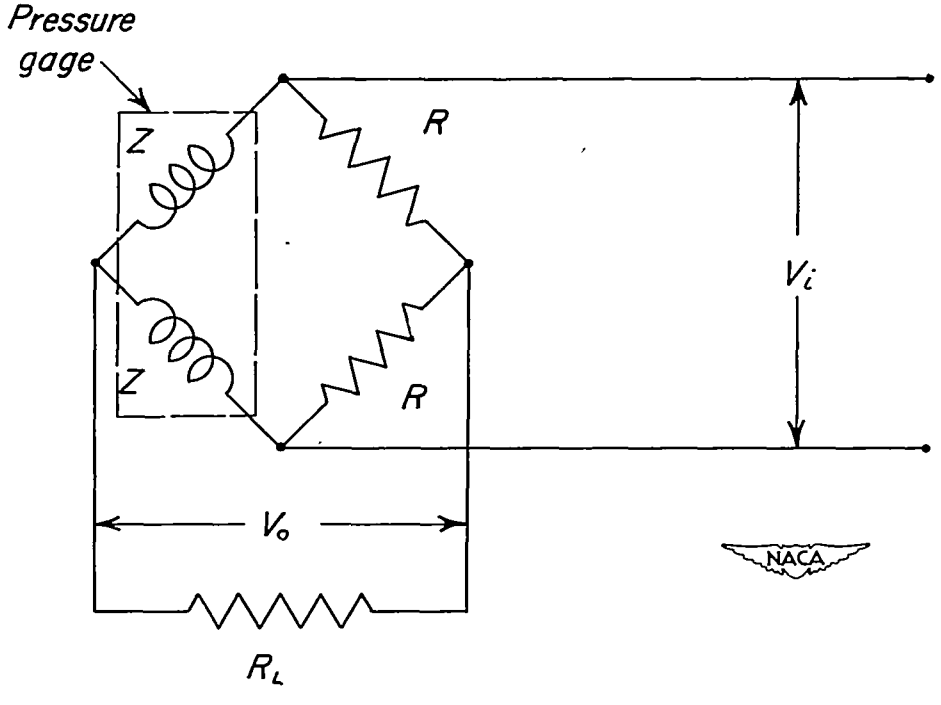

Figure 8.- Simplified alternating-current bridge circuit showing symbols used in this paper.

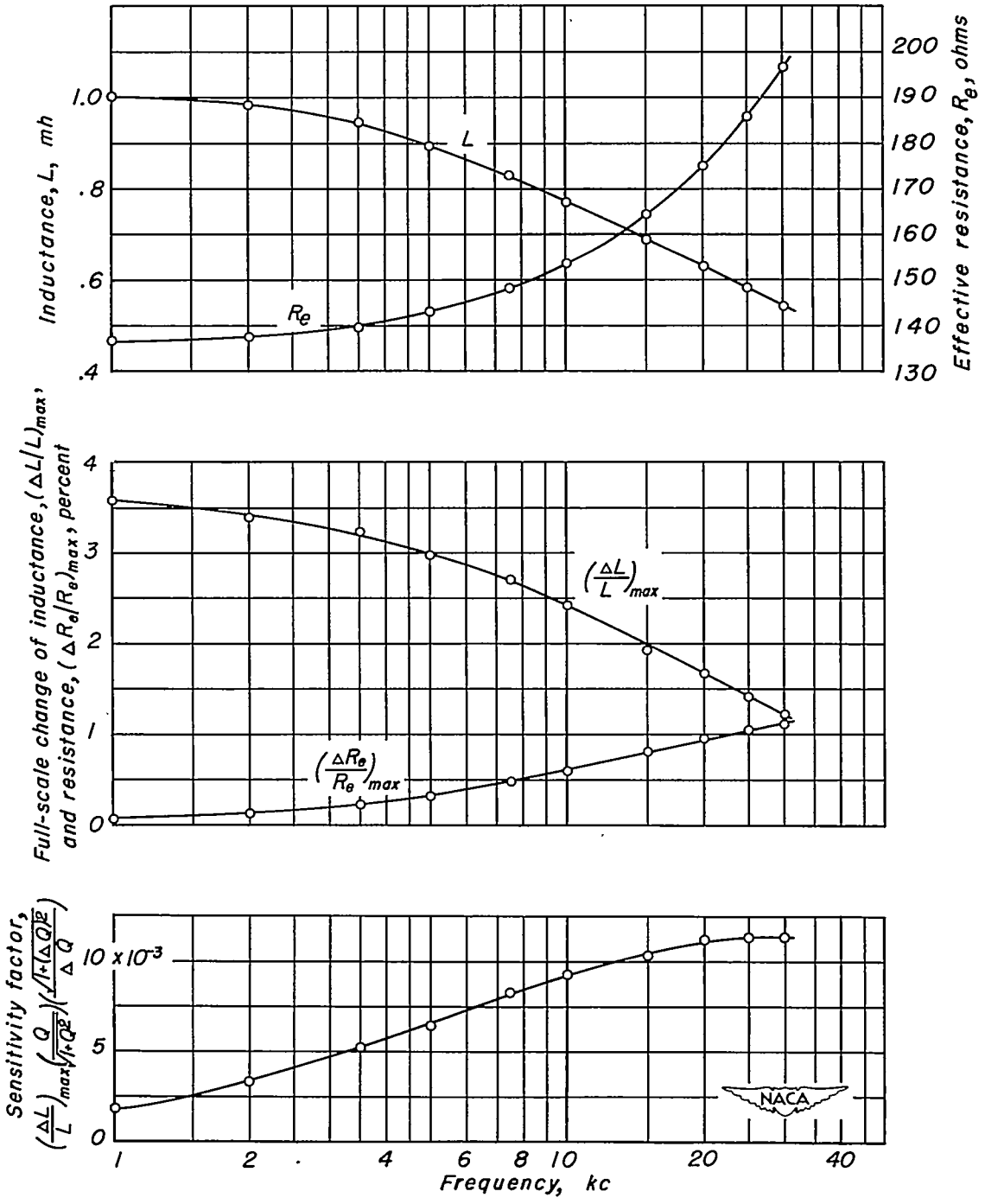

Figure 9.- Various properties of a typical coil of an NACA miniature electrical pressure gage as determined by measurements using an Anderson bridge with 1 volt impressed on the coil.

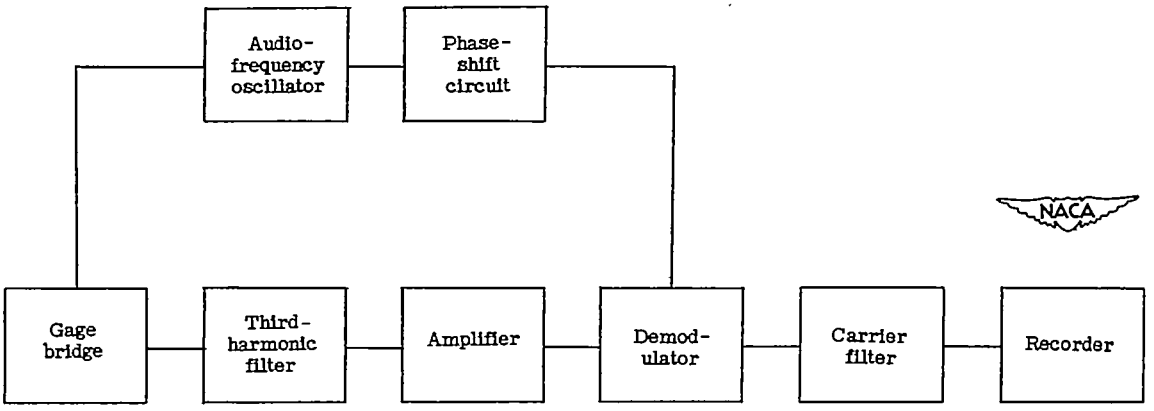

Figure 10.- Block diagram of the carrier equipment normally used with inductance-type gages.

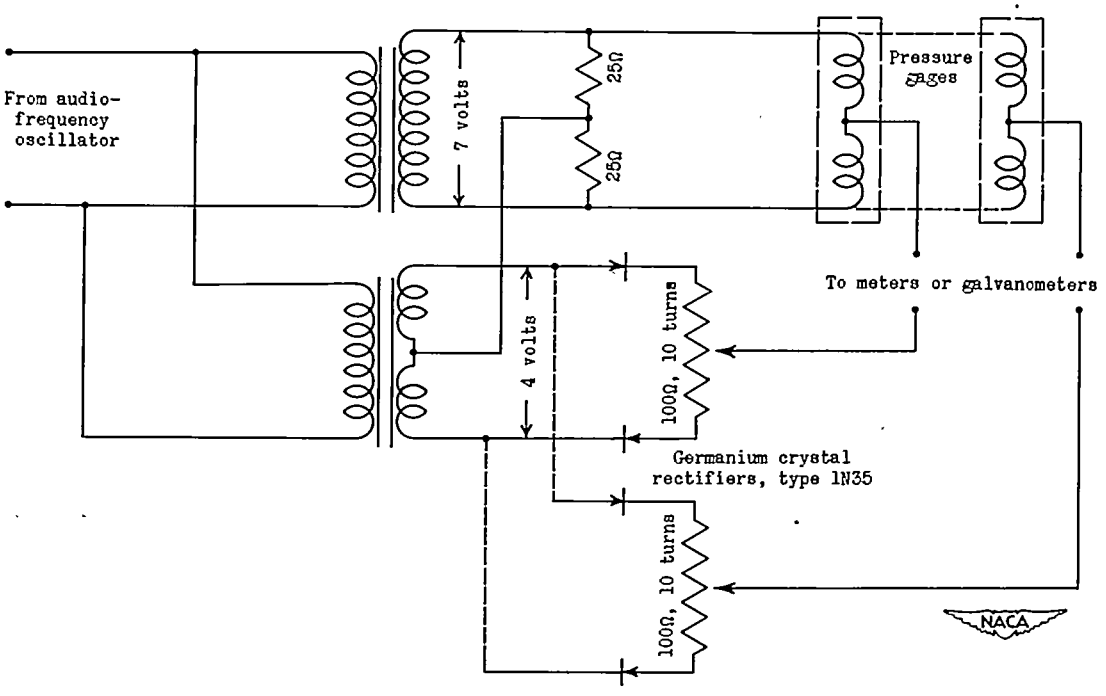

Figure 11.- Multichannel circuit employing direct demodulation and used to drive sensitive galvanometers.

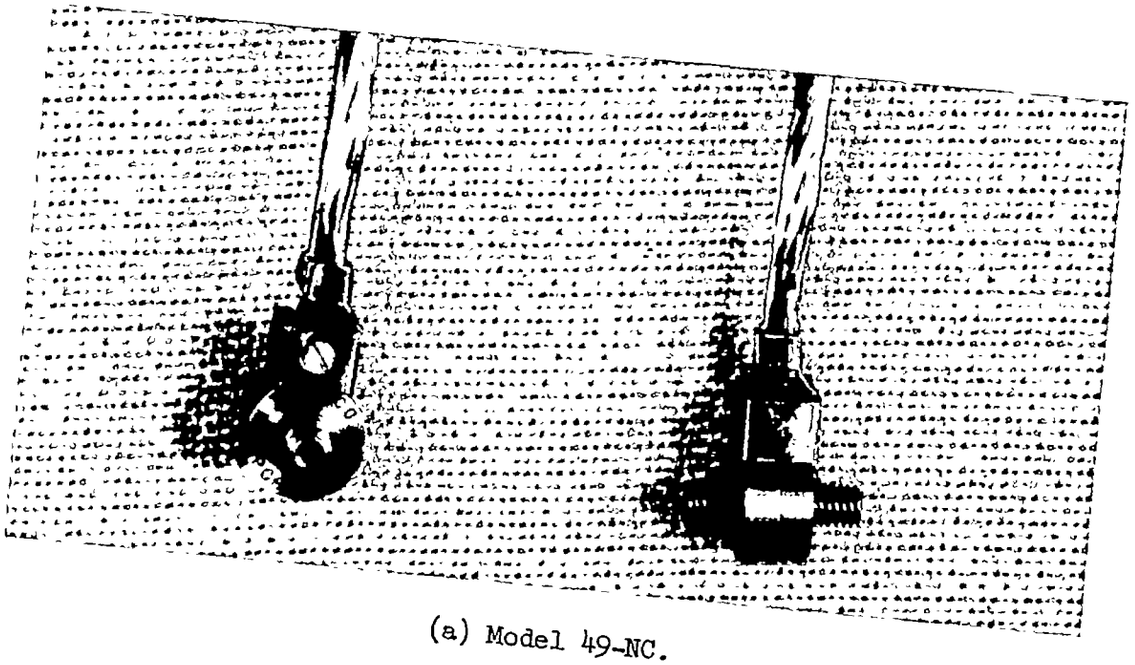

(a) Model 49-NC.

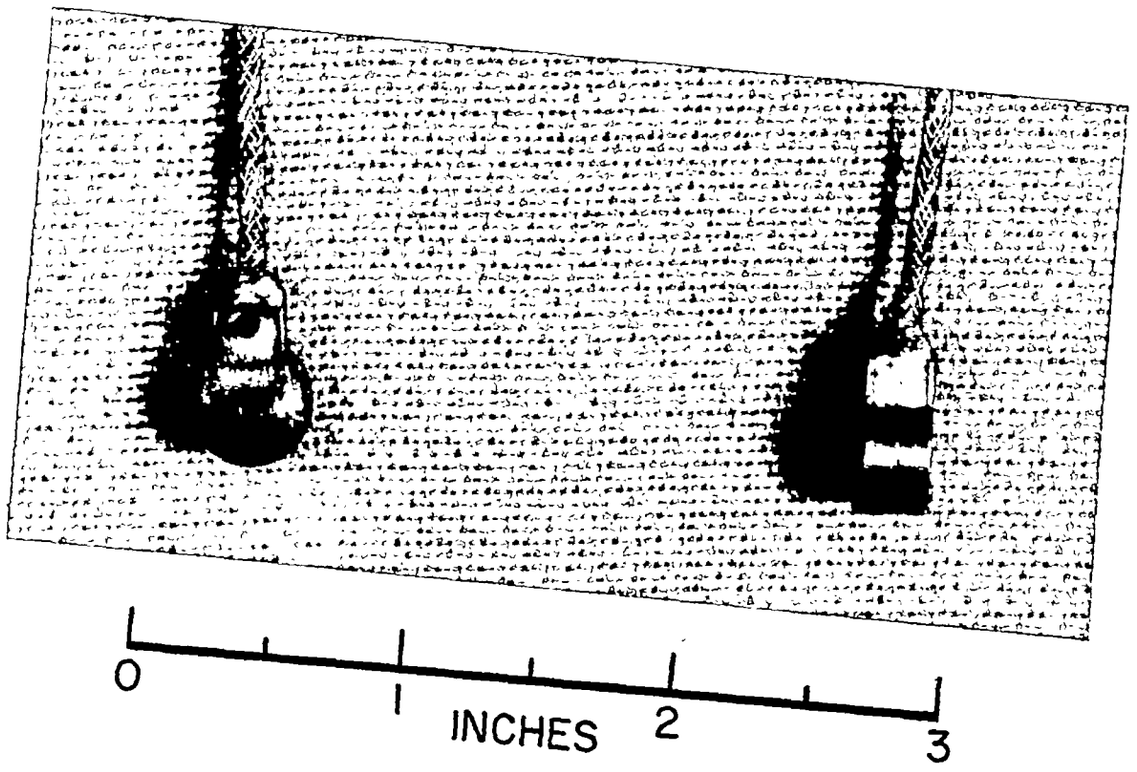

(b) Model 49-TP.

NACA L-72707

Figure 12.- The two most widely used models of the NACA miniature electrical pressure gage.

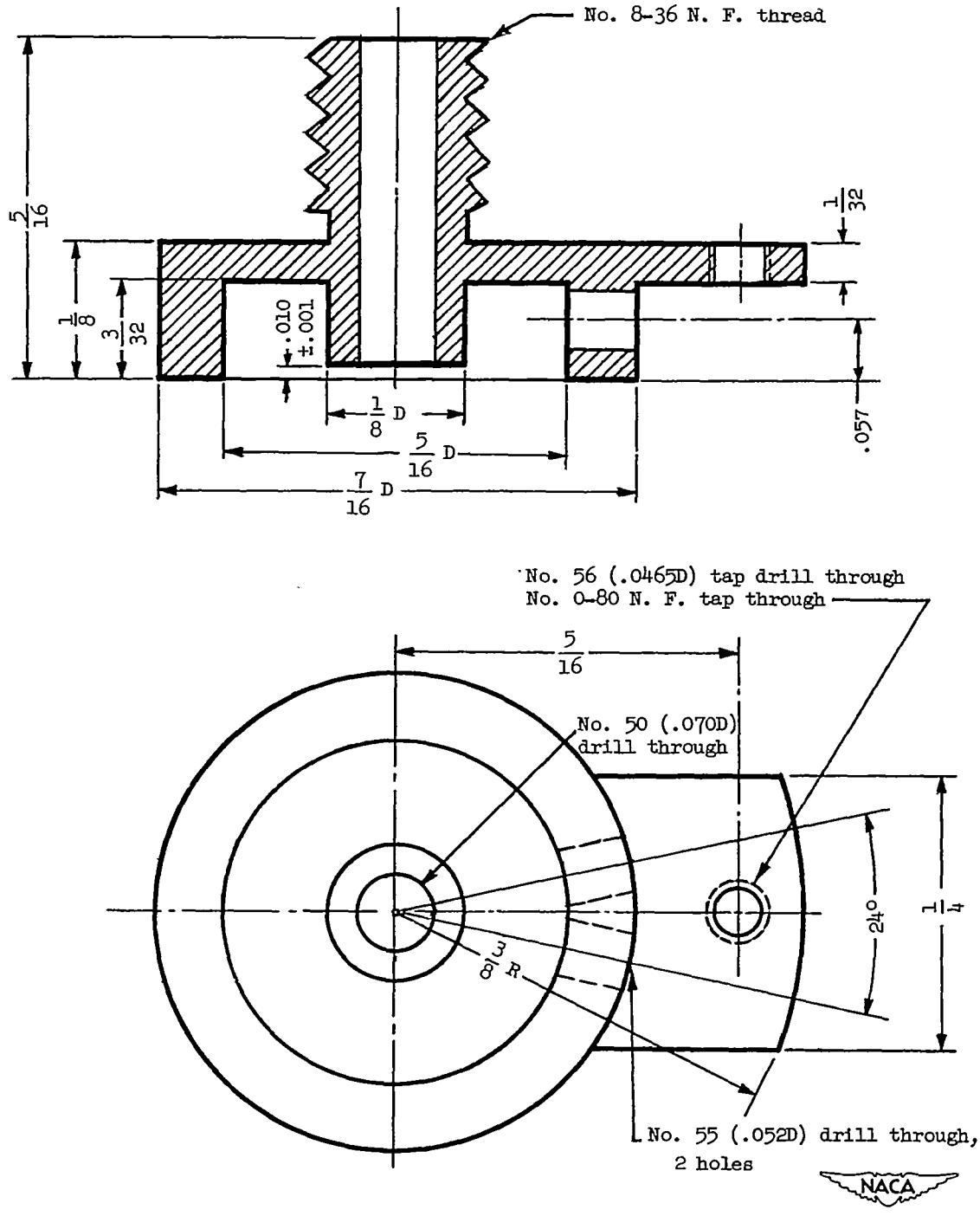

(a) Case. 42-percent nickel, 58-percent iron alloy. Two required.

Figure 13.- Detailed drawings of the main components of the NACA miniature electrical pressure gage model 49-NC. (Notations are in accordance with standard drafting practice.)

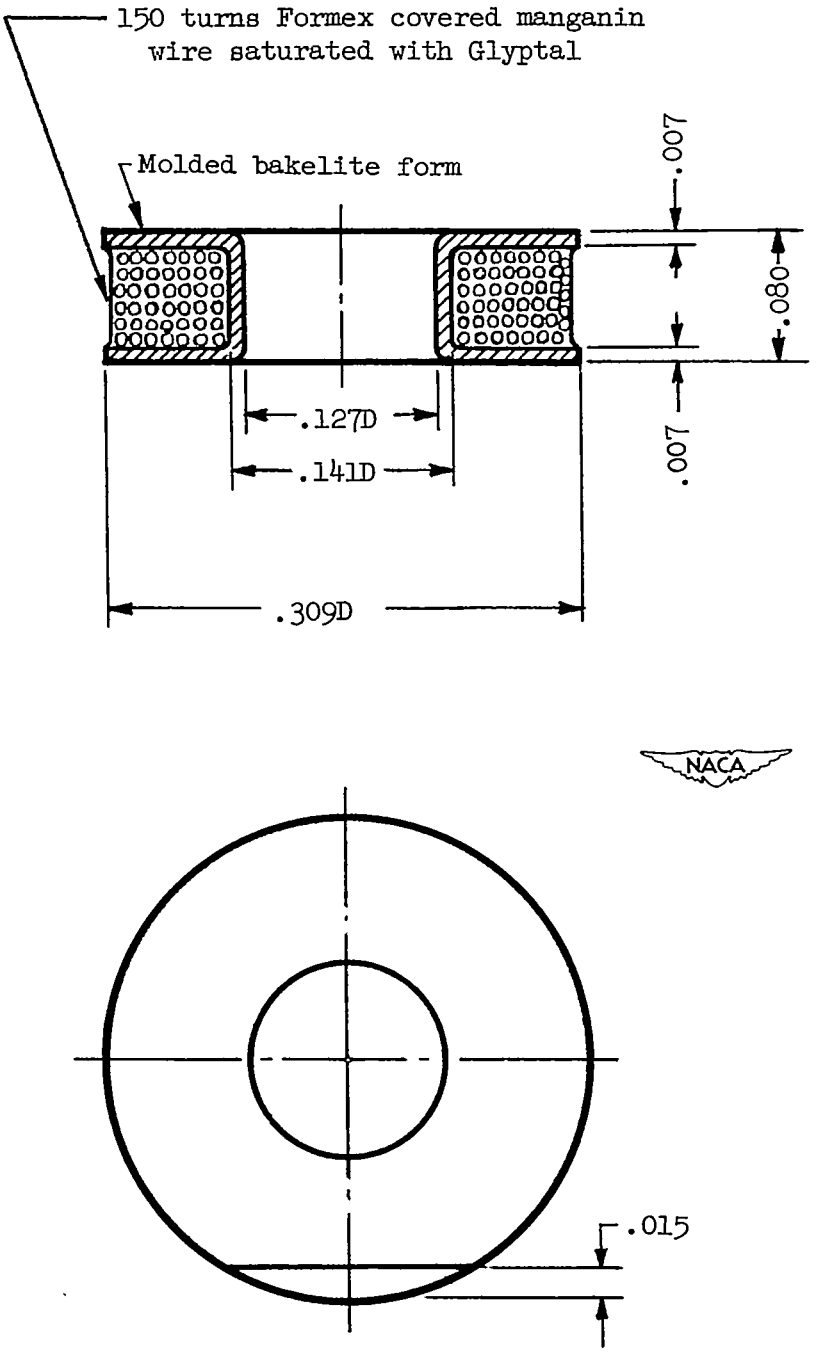

(b) Coil. Two required.

Figure 13.- Continued.

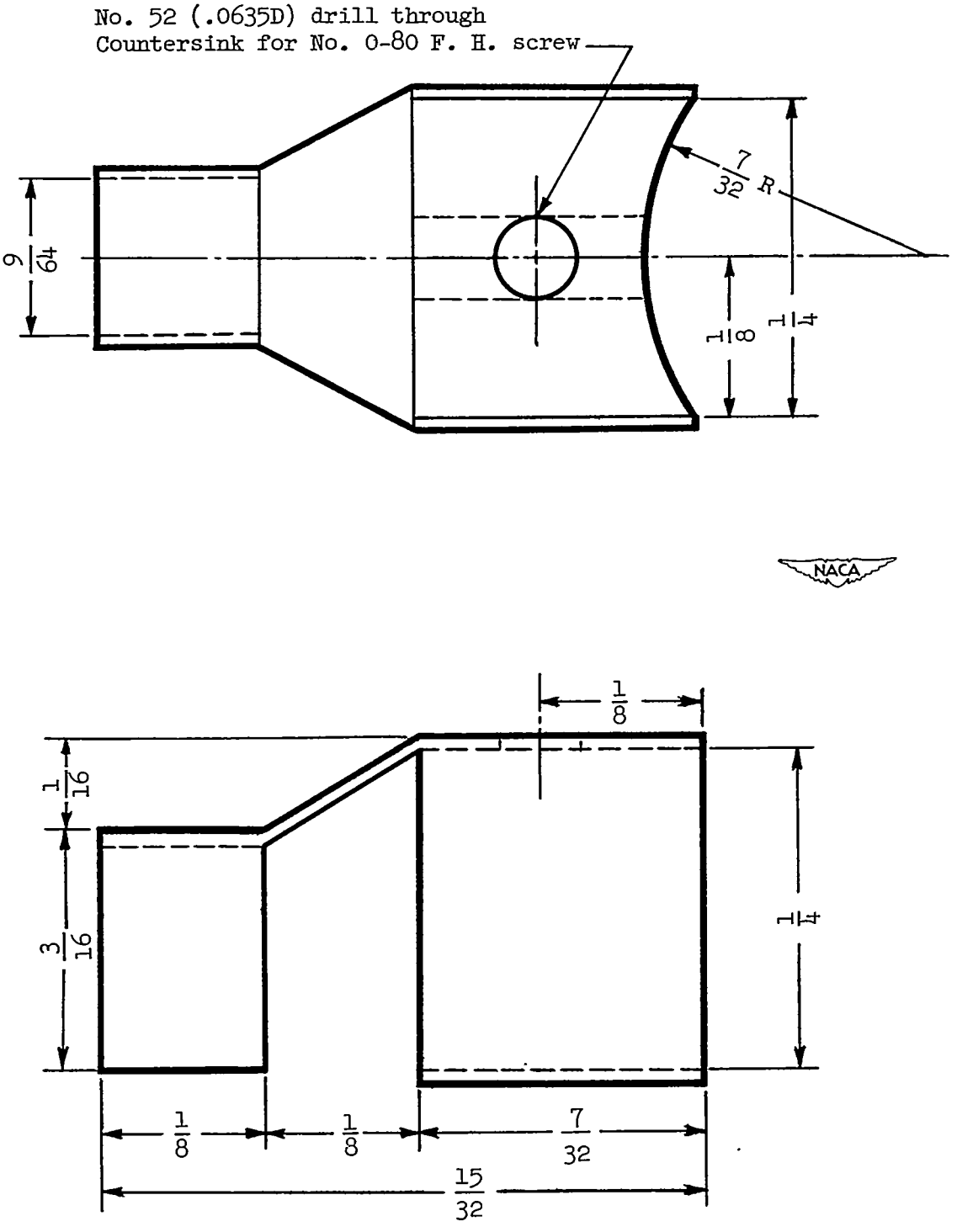

(c) Cable clamp. 28-gage stainless steel.

Figure 13.- Concluded.

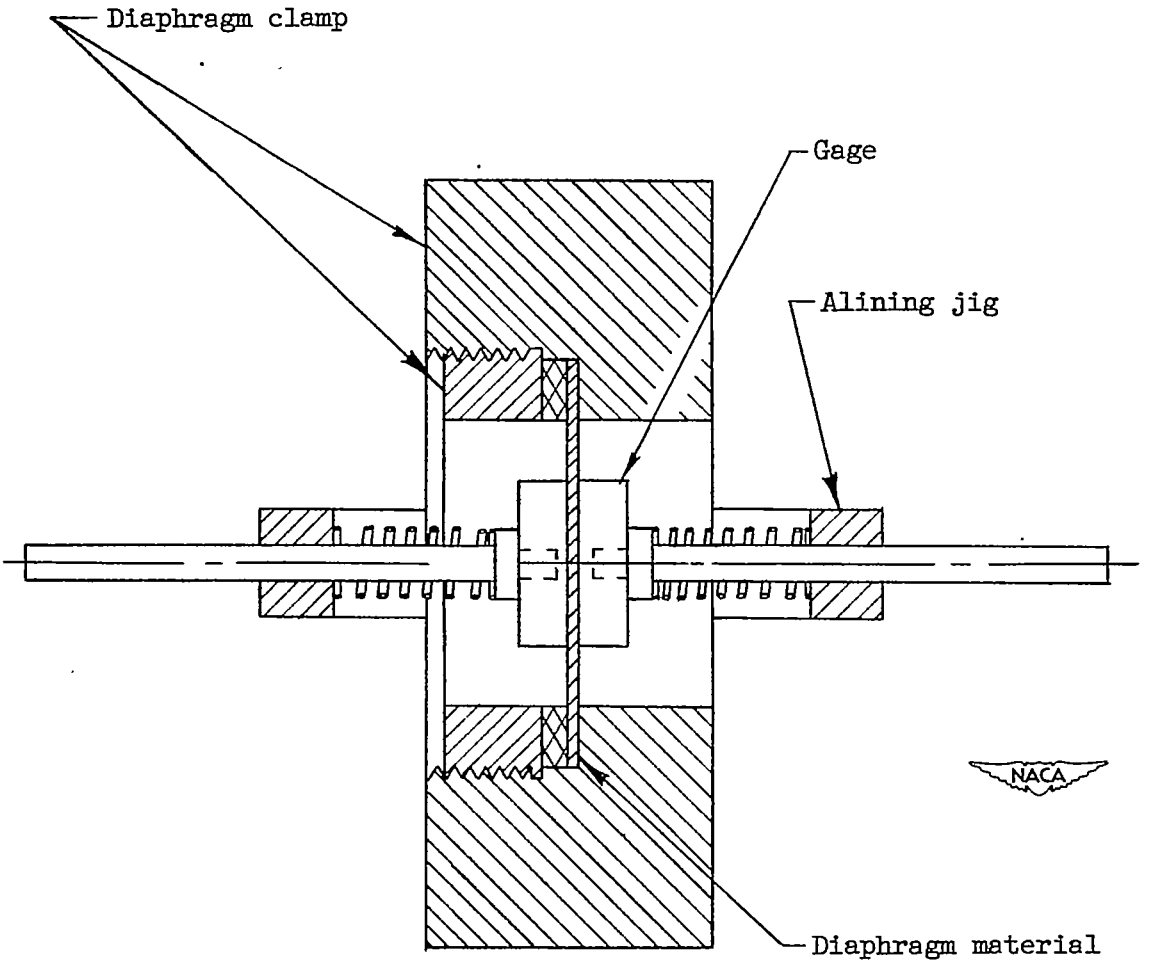

Figure 14.- Sketch of the soldering jig used when stretching and soldering the diaphragms.

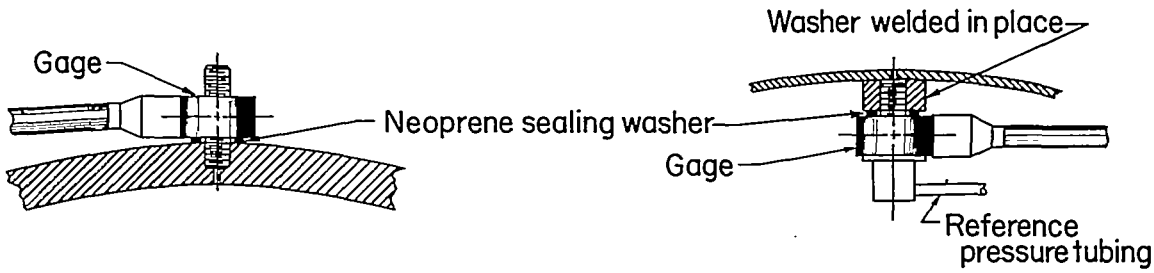

(a) Tunnel wall and so forth. (b) Skin of model and so forth.

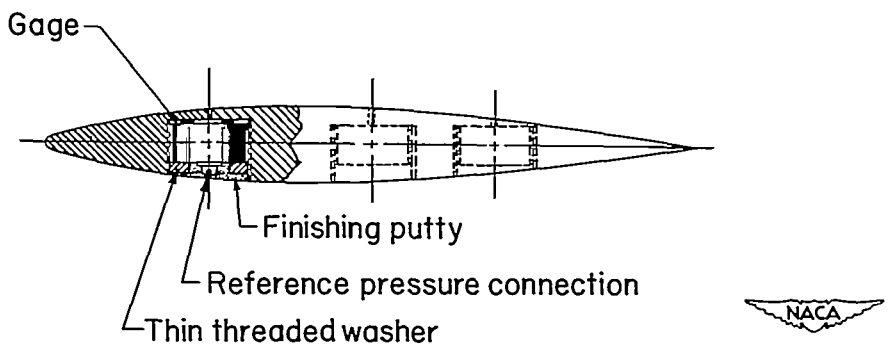

(c) Small solid airfoil.

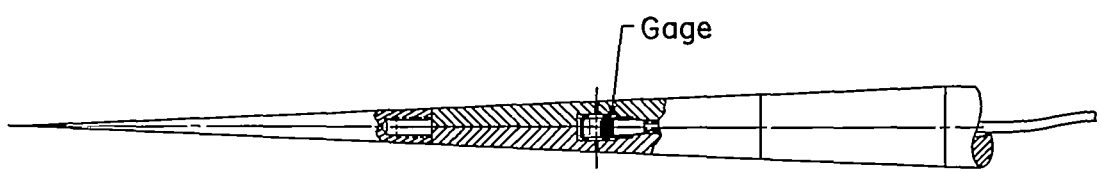

(d) Conical supersonic survey probe.

Figure 15.- Sketches showing typical installations of the NACA miniature electrical pressure gage.

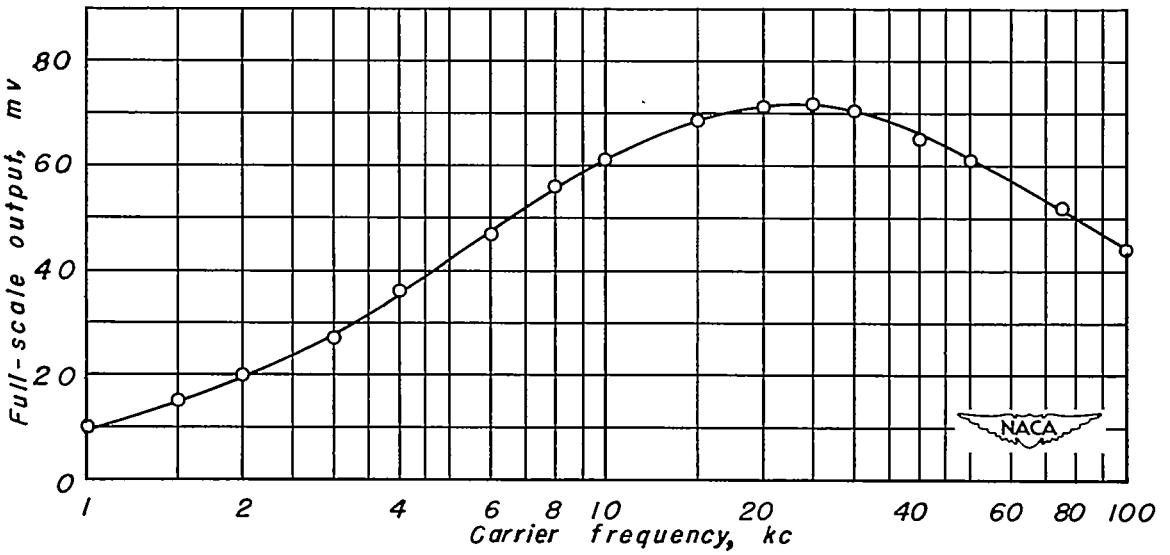

Figure 16.- Full-scale voltage output as a function of carrier frequency for a typical 15-pound-per-square-inch miniature pressure gage, when using the bridge circuit of figure 17.

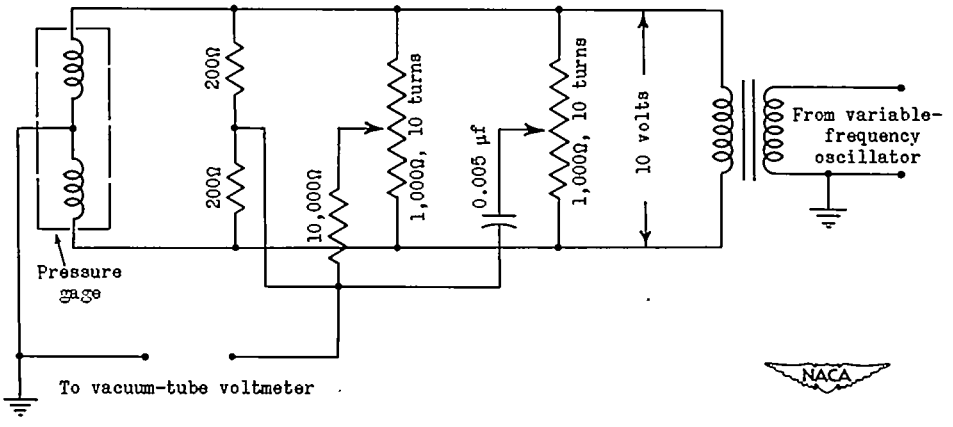

Figure 17.- Typical inductance-gage bridge circuit.

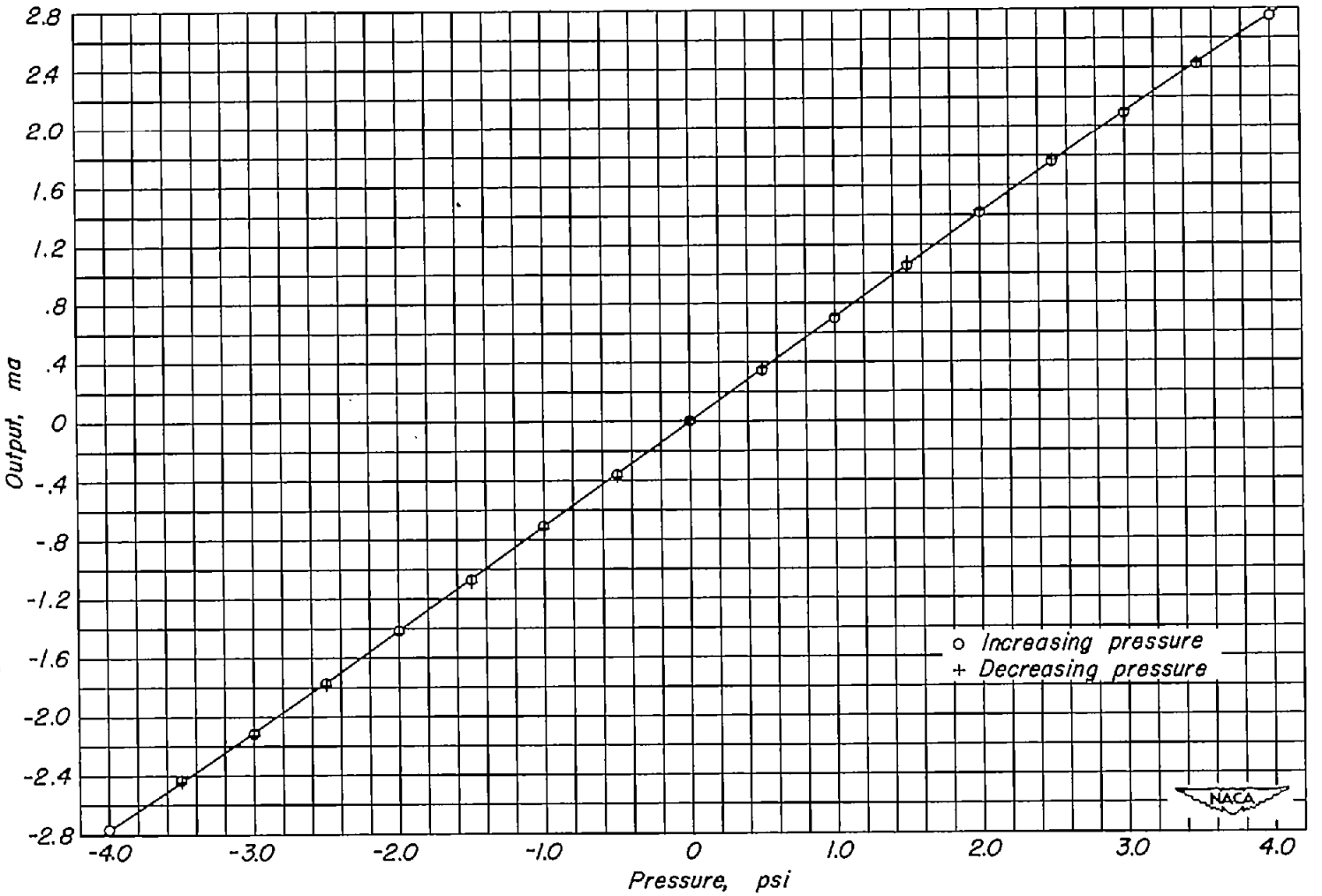

Figure 18.- Calibration curve of a typical 4-pound-per-square-inch miniature pressure gage when using a commercial carrier amplifier system.

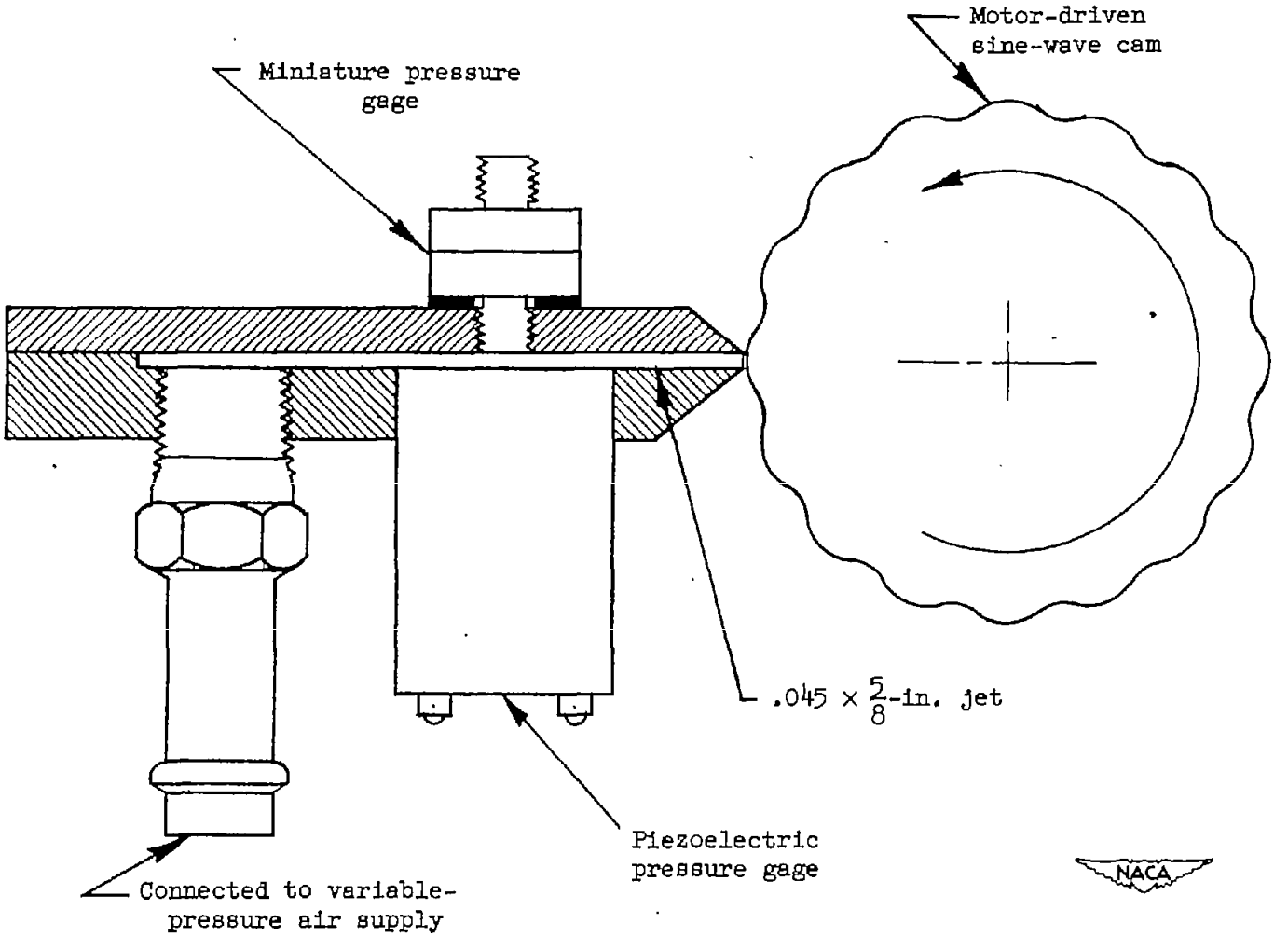

Figure 19.- Sketch of pressure pulsator used to check the frequency response of dynamic-pressure gages.

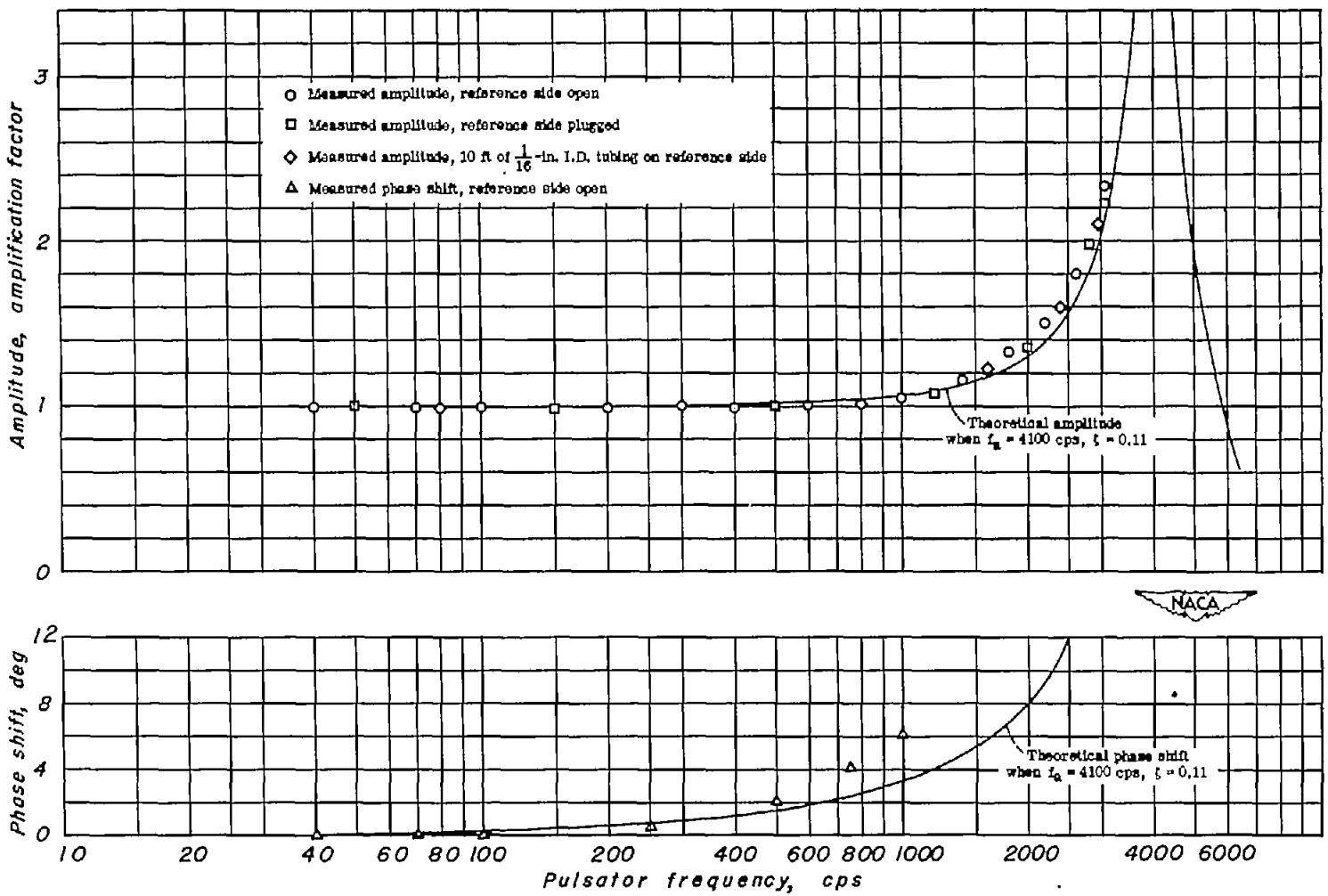

Figure 20.- Frequency-response calibration of a typical 8-pound-per-square-inch NACA miniature electrical pressure gage model 49-NC with no added tubing.

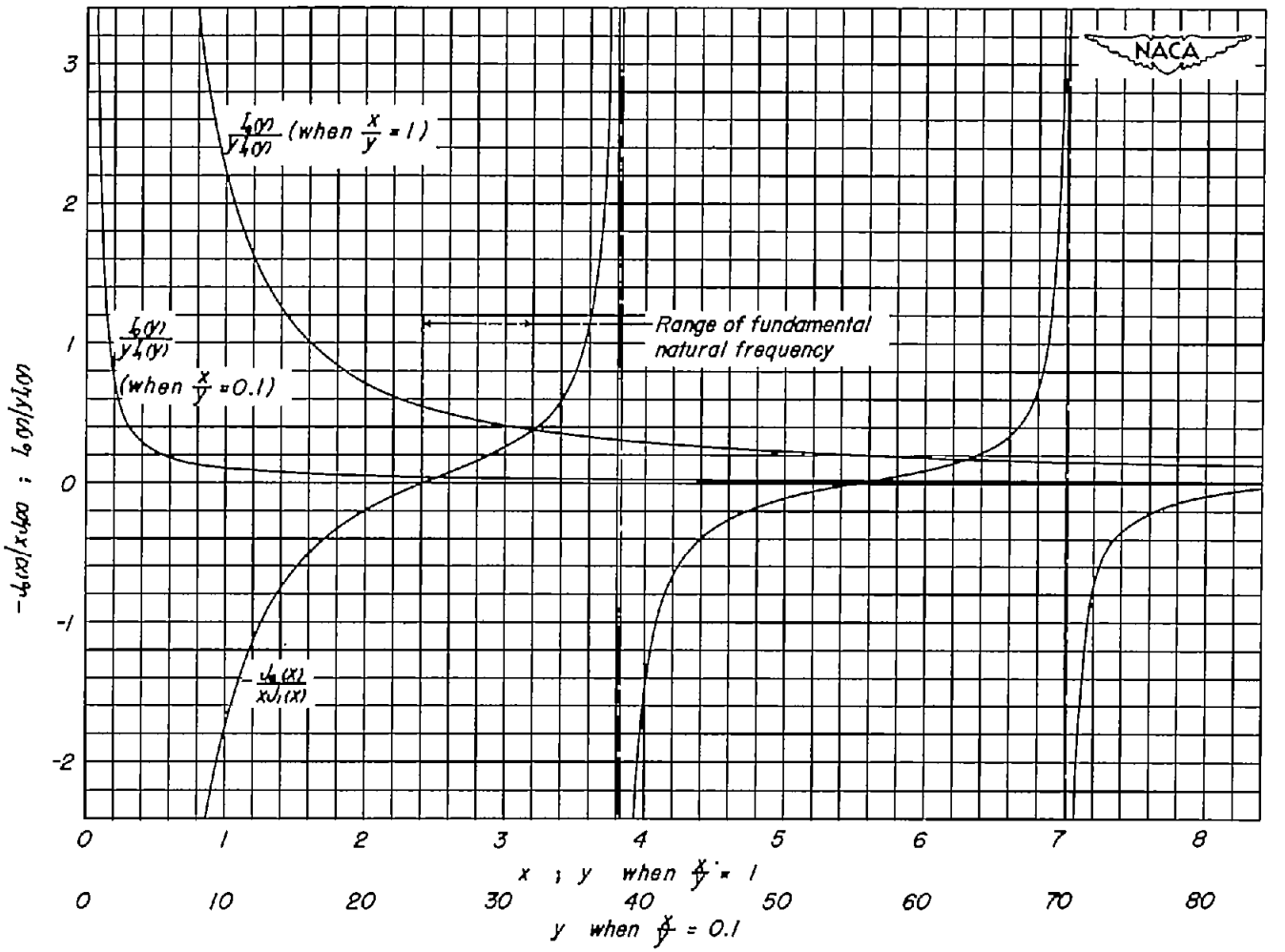

Figure 21.- Graphical solution of equation (A2) for the particular cases where $\frac{x}{y} = 1$ and $\frac{x}{y} = 0.1$.